Journal of Computational Physics 406 (2020) 109183

Contents lists available at ScienceDirect

Journal of Computational Physics

www.elsevier.com/locate/jcp

A discontinuous Galerkin method for the Aw-Rascle traffic flow model on networks

Joshua Buli [a,1], Yulong Xing [b,*,2]

[a] Department of Mathematics, University of California Riverside, Riverside, CA 92521, USA
[b] Department of Mathematics, Ohio State University, Columbus, OH 43210, USA

ARTICLE INFO

Article history:
Received 2 February 2019
Received in revised form 16 October 2019
Accepted 11 December 2019
Available online 19 December 2019

Keywords:
Discontinuous Galerkin method
Hyperbolic conservation laws on networks
Aw-Rascle model
Traffic flow
High order method

ABSTRACT

Macroscopic models for flows strive to depict the physical world by considering quantities of interest at the aggregate level versus focusing on each discrete particle in the system. Many practical problems of interest such as the blood flow in the circulatory system, irrigation channels, supply chains, and vehicular traffic on freeway systems can all be modeled using hyperbolic conservation laws that track macroscopic quantities through a network. In this paper we consider the latter, specifically the second-order Aw-Rascle (AR) traffic flow model on a network, and propose a discontinuous Galerkin (DG) method for solving the AR system of hyperbolic partial differential equations with appropriate coupling conditions at the junctions. On each road, the standard DG method with Lax-Friedrichs flux is employed, and at the junction, we solve an optimization problem to evaluate the numerical flux of the DG method. As the choice of well-posed coupling conditions for the AR model is not unique, we test different coupling conditions at the junctions. Numerical examples are provided to demonstrate the high-order accuracy, and comparison of results between the first-order Lighthill-Whitham-Richards model and the second-order AR model. The ability of the model to capture the capacity drop phenomenon is also explored.

1. Introduction

Macroscopic continuum models for hyperbolic network flows have been applied in a diverse array of applications in a variety of scientific fields. Such models utilize partial differential equations (PDEs) to simulate the evolution of the macroscopic quantities across a network. The practicality of the macroscopic PDE methods is realized through the simulation of large networks with many junctions and edges. A large network poses computational time issues if microscopic models are used, as the behavior of each entity across the network must be taken into account. Applications of hyperbolic network flows include blood circulation [29,34], supply chains [4], data packet flow and telecommunications [20], air traffic management [39], vehicular traffic flow [2], and many more. A comprehensive overview of hyperbolic flows on networks is given in [10], which provides theoretical results, models for various types of applications of network flows, coupling conditions, and some numerical results.

* Corresponding author.
E-mail addresses: jbuli001@ucr.edu (J. Buli), xing.205@osu.edu (Y. Xing).

[1] The work of this author was partially supported by the National Center for Sustainable Transportation (NCST) Graduate Fellowship and the NSF grant CMMI-1629195.
[2] The work of this author was partially supported by the NSF grant DMS-1753581 and ONR grant N00014-16-1-2714.

https://doi.org/10.1016/j.jcp.2019.109183
0021-9991/

The spatial component of the model is given by a network, or topological graph, consisting of a collection of edges (also called links) and a set of junctions (also called nodes or vertices). Edges are connected at junctions, along with additional requirements so that the network can be described mathematically as a graph. On each edge, the dynamics are described by solutions to either a scalar PDE or systems of PDEs. As this paper is concerned with the application of traffic flow, terminology from traffic flow literature will be employed. A *first-order model* is a model where the evolution of vehicle density on the network are given by a single PDE on each edge. A *second-order model* is a model in which the dynamics are governed by a system of two PDEs on each edge, one for the density and one for the velocity of vehicles. This notion can be extended to larger systems as well. The use of the word "high-order" should not be confused with the terminology of the numerical analysis community, where a "high-order method" is a numerical scheme that can achieve a high-order of accuracy for computational implementation.

Much theoretical work has been done studying first and second order models of traffic flow. The seminal work done by Lighthill and Whitham [27] and Richards [36] developed the first order model for traffic flow, now known as the Lighthill-Whitham-Richards (LWR) model of traffic flow, describing evolution of traffic density over time. The LWR model can be written in conservative form as

$$\partial_t u + \partial_x f(u) = 0, \tag{1.1}$$

where $f(u) = uv(u)$ represents the flow of vehicles, and u and v are the vehicle density and velocity, respectively. Eq. (1.1) is also known as the continuity equation, and states that the number of vehicles is to be conserved. The average velocity function $v = v(u)$ is a decreasing function of the density u, and the flow function $f(u) = uv(u)$ defines a unique relationship between flow and density and is termed the "macroscopic fundamental diagram" (MFD) of traffic flow. Much work has been done on developing different MFDs, as well as showing that MFDs fit experimental data [19]. For our paper we are primarily interested in the numerical aspects of the junction problem, so when the LWR model is considered we simply take the normalized Greenshields' relation $v(u) = 1 - u$, which states that velocity is a negative linear function of density, so that the flux becomes $f(u) = u(1-u)$. In the 1990s, Daganzo [16] developed the cell-transmission model (CTM) for the first order traffic flow problem, which looks at discrete vehicles in a discretized road, and proved that in the limit, the CTM approaches the first order LWR model. In [18], the method was extended to the network case. Also in 1995, Holden and Risebro [25] developed theory for the first order model on a network.

Second-order models were developed in an attempt to improve upon the first-order LWR model. In 1971, Payne [33] derived a second-order model, using fluid flow as a basis for the extension. The model included a second PDE which made the velocity dynamic. This is due to certain limitations of using a single conservation law as in (1.1) to model the dynamics of traffic congestion, especially traffic jam situations, where decreased flow is observed on a traffic network when density rises above a critical value. The analogy of treating traffic as a fluid was advanced to use high-order models from fluid dynamics to add more details to traffic models, but the analogy between traffic flow and fluid flow is imperfect. In [17], Daganzo provided strong criticism against second-order models of traffic flow up to 1995, as the motion of fluid particles are determined by information both in front of and behind the particle, while traffic flow is anisotropic in nature, in that the driver is only influenced by the conditions downstream from its current position.

Aw and Rascle [5] developed a "proper" second-order model of traffic flow which addressed the criticisms of Daganzo [17] that the existing second order models were non-physical. The model is a nonlinear hyperbolic system of PDEs, which we will refer to as the Aw-Rascle (AR) model, and is given by

$$\begin{cases} \partial_t u + \partial_x (uv) = 0 \\ \partial_t (u(v + p(u))) + \partial_x (uv(v + p(u))) = 0, \end{cases} \tag{1.2}$$

where $u(x,t)$ and $v(x,t)$ represent the density and velocity of the vehicles, respectively. The function $p(u)$ is the "pressure" term, which is taken as an increasing function of the density u. The pressure is a well defined quantity in fluid flow, but may seem inappropriate for traffic flow, as there is not an immediate physical intuition of what pressure would represent. In fact, in [5], the authors state that the pressure term describes how drivers react to a change in the concentration of vehicles in front of them. Thus the pressure function is often referred to as an "anticipation" factor. For our numerical work, we take the pressure function to have the form $p(u) = u^\gamma$, which is a common assumption in inviscid fluid flow theory. The adiabatic constant, γ, is generally taken such that $\gamma > 1$. We can rewrite (1.2) as

$$\begin{cases} \partial_t u + \partial_x (q - up(u)) = 0 \\ \partial_t q + \partial_x \left(\dfrac{q^2}{u} - qp(u) \right) = 0, \end{cases} \tag{1.3}$$

where $q = u(v + p(u))$ represents a "pseudo-momentum". For the numerical work in this paper, we will utilize the conservation form[3] of the AR model given by (1.3). We are interested in the network problem corresponding to the AR model,

[3] We could also write (1.3) in system form $U = (u, q)^T$, which will be done in (3.4). The notation, U, will be used to define the coupling conditions in a concise way.

which will be described in detail in Section 2. A traffic network consists of edges, in this case roads, that meet at a single node (junction), where the dynamics on each road are given by (1.3), and some prescribed conditions are defined at the junction, which are termed coupling conditions. We only consider single junction cases, with a particular number of incoming and outgoing roads with one node. As the propagation speeds of the waves is finite, our method can be extended to multiple junctions by combining the junction types together to form a complex network.

There has also been a wide variety of work done on the numerical analysis of hyperbolic network flows across different fields. Applications where numerical methods have been employed to solve hyperbolic flows on networks include shallow water equations in channels [11,7], gas dynamics [6], blood flow circulation [29], and first order traffic flow models [2]. In particular, the discontinuous Galerkin (DG) method is applied to the first order LWR model on a network in [2], where the Riemann problem is solved exactly to determine the coupling conditions, and an equivalent form of the Godunov flux is applied to solve the junction problem. Other numerical methods using different approaches have been developed for traffic flow models including the cell transmission model [16], finite difference methods [28], WENO schemes for the multi-class LWR model [40], and finite volume methods for the Aw-Rascle-Zhang model [37].

In the past 20 years, high order accurate numerical schemes have gained increased attention and are being applied in many computational fields where systems of conservation laws appear. Among the choices of high-order methods, the DG method is a class of finite element methods that uses completely discontinuous piecewise polynomial basis functions, which reaps the benefits from both finite element and finite volume methods (see [35,14,15,12], and [13] for a historic review). The DG method holds many superior advantages, including the local conservativity, the easy handling of complicated geometries, simple implementation boundary conditions, the implementation of *hp*-adaptivity, and highly efficient parallel implementations. DG methods have attracted increased attention for applications requiring high performance computing in large scale problems. Parallel efficiencies have been shown to be more than 80% for adaptive meshes and more than 99% for fixed meshes [8]. The DG method also provides simple adaptation with the predominantly used finite volume techniques, which benefits those groups who already implement those methods. These make the use of the DG method quite promising for the traffic flow problems on networks considered in this paper.

In the present paper, we discuss the derivation and development of DG methods to solve the Aw-Rascle model (1.3) on a network with various junction types and different coupling conditions. In [2], DG methods with Godunov flux are presented to solve the LWR model on networks. The Godunov flux, based on the exact Riemann solution, is computed at the junction, which relies on multiple cases for each type of junction. The number of cases also increases with the number of roads, thus making the evaluation of the flux at the junction complicated and time consuming if there are many roads entering and leaving the junction. Also, when the second order AR model is considered in this paper, it becomes too complicated to solve the Riemann problem exactly at the junction to determine the numerical flux. In [9], a first order numerical algorithm is developed to solve the coupling conditions at a junction via an optimization problem, and the accuracy and effectiveness of this algorithm is validated for the shallow water equations on networks. In this paper, we combine this technique with the DG methods and introduce a high order algorithm which can efficiently solve the AR model on networks. At the junction, only a single optimization problem, based on the DG solutions of directly neighboring cells on each road, needs to be solved with the *a priori* coupling conditions which can be handled by built-in solvers. One attraction of this formulation is that we can use fluxes other than the Godunov flux, say the Lax-Friedrichs flux or FORCE scheme, which do not require the exact solution of the Riemann problem. The novel contribution of this work is to introduce a high order DG framework for the AR traffic flow system which allows the usage of any numerical flux. The DG method allows for easy handling at the junction, as the method only relies on information from directly neighboring cells, making it an ideal choice for the junction problem. It was emphasized in [2] that "the DG method perhaps is the only realistic and efficient high order method for network problems".

The organization of the paper is as follows. Section 2 presents a detailed description of the network problem, along with choices of coupling conditions at the junction. In Section 3, we present a DG method for the network problem given in Section 2. The detailed implementation of the coupling conditions at the junction is presented in Section 4. Section 5 contains various numerical experiments that show the optimal convergence rates, comparisons of different coupling conditions, and the behavior of the second order model. As comparison, we also implement the first order LWR model on networks with DG methods using Godunov flux, and the comparison of LWR and AR models on networks with the proposed DG method is also provided. We also compare how different coupling conditions affect the numerical scheme for the AR model. In addition, we present numerical results to show the capacity drop effect at the junction for two incoming roads and one outgoing road. Finally, concluding remarks are given in Section 6.

2. Aw-rascle traffic flow on a network

The introduction provided the history of the theoretical aspects of traffic flow modeling. In this section, a brief review of the AR traffic flow model on a network is given. In section 2.1 we define the problem of interest, the network AR model and notational conventions that will be important for the remainder of the paper. Section 2.2 outlines the theoretical work that has been done in developing coupling conditions that satisfy the Riemann problem at the junction.

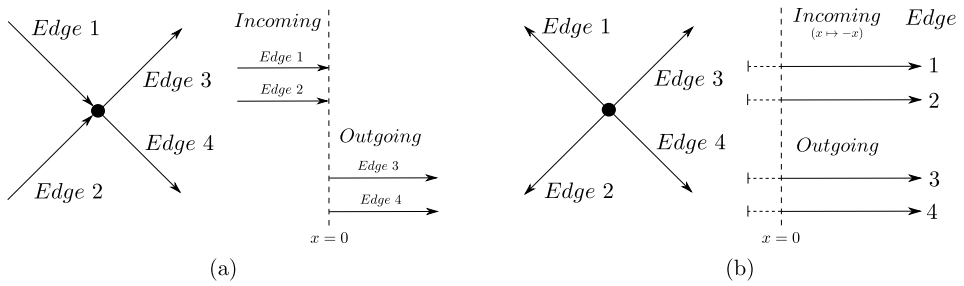

Fig. 2.1. Notation at the junction. (a) The left subfigure of (a) gives the direction of traffic where the arrows that point to the vertex (Edges 1 and 2) represent incoming roads, and the arrows pointing away from it are outgoing roads, for the case of 2 incoming roads and 2 outgoing roads. This notation is used in [21]. The right subfigure of (a) gives the junction in terms of the interface, where the vertex represents $x = 0$. (b) The left subfigure of (b) gives the situation after the $x \mapsto -x$ has been applied to the incoming roads, so the direction of all traffics points outwards from $x = 0$. In the right subfigure of (b), each road points out of the vertex at $x = 0$, where the dotted line to left represents the "ghost cell". This notation is used in [9].

2.1. Notation and conventions

In this subsection, we give concrete definitions and notational conventions that will hold for the remainder of the paper. In [21] and [25], the notational convention gives the following definition for incoming and outgoing roads. Each road k is described as the interval $[a_k, b_k]$ where $a_k = -\infty$, $b_k = 0$ for incoming roads, and $a_k = 0$, $b_k = +\infty$ for outgoing roads. They assume that traffic goes in the direction from a_k to b_k, thus traffic has positive speed in that direction. This notational convention can be visualized in Fig. 2.1a, where the vertex diagram and interface diagram provide a visual of the junction.

An alternative way to represent the roads, used in [9], utilizes a position mapping $x \mapsto -x$ to the incoming road. The mapping allows the incoming roads to be represented on a positive interval, so that all roads are directed out of the interface at $x = 0$. To simplify the situation further for the numerical work, we consider each road on the unit interval $[0, 1]$, exiting the junction. Each road has a dotted line portion to the left of the junction which represents a "ghost cell" for the solution of the left state of the Riemann problem at the junction. This notational convention can be visualized in right subfigure of Fig. 2.1b. For the remainder of the paper, we will use the notational convention in Fig. 2.1b on the unit interval.

For the traffic network problem, we apply the AR model given by (1.3), on each road. Assume that there are a total of m roads, so that initial conditions $u_0^{(k)}(x)$ and $q_0^{(k)}(x)$ are prescribed on each road $k = 1, \dots, m$. Let there be $\widetilde{m}$ incoming roads and $\widehat{m}$ outgoing roads such that $m = \widetilde{m} + \widehat{m}$. We must also provide coupling conditions at the junction, denoted as $\Phi(U^{(1)}(t, 0^+), \cdots, U^{(m)}(t, 0^+)) = 0$, where $U = (u, q)^T$ denotes the vector of unknown variables. The coupling conditions describe how traffic moves from incoming roads to outgoing roads at the interface. Putting together (1.3), the initial conditions, and coupling conditions, we can describe the AR traffic network model on outgoing roads as

$$\begin{cases} \partial_t u^{(k)}(t,x) + \partial_x \left(q^{(k)}(t,x) - u^{(k)}(t,x) p(u^{(k)}(t,x)) \right) = 0 & (t,x) \in \mathbb{R}^+ \times [0,1],\ k = \widetilde{m}+1, \dots, \widetilde{m}+\widehat{m} \\ \partial_t q^{(k)}(t,x) + \partial_x \left(\dfrac{(q^{(k)}(t,x))^2}{u^{(k)}(t,x)} - q^{(k)}(t,x) p(u^{(k)}(t,x)) \right) = 0 & \\ \begin{cases} u^{(k)}(0,x) = u_0^{(k)}(x) & \text{for } x \in [0,1] \\ q^{(k)}(0,x) = q_0^{(k)}(x) & \text{for } x \in [0,1] \\ \Phi(U^{(1)}(t,0^+), \cdots, U^{(m)}(t,0^+)) = 0 & t \geq 0, \end{cases} & \end{cases} \tag{2.1}$$

and incoming roads as

$$\begin{cases} \partial_t u^{(k)}(t,x) - \partial_x \left(q^{(k)}(t,x) - u^{(k)}(t,x) p(u^{(k)}(t,x)) \right) = 0 & (t,x) \in \mathbb{R}^+ \times [0,1],\ k = 1, \dots, \widetilde{m} \\ \partial_t q^{(k)}(t,x) - \partial_x \left(\dfrac{(q^{(k)}(t,x))^2}{u^{(k)}(t,x)} - q^{(k)}(t,x) p(u^{(k)}(t,x)) \right) = 0 & \\ \begin{cases} u^{(k)}(0,x) = u_0^{(k)}(x) & \text{for } x \in [0,1] \\ q^{(k)}(0,x) = q_0^{(k)}(x) & \text{for } x \in [0,1] \\ \Phi(U^{(1)}(t,0^+), \cdots, U^{(m)}(t,0^+)) = 0 & t \geq 0, \end{cases} & \end{cases} \tag{2.2}$$

where $u^{(k)}(t,x)$ and $q^{(k)}(t,x)$ are the density and pseudo-momentum on the kth road, and the fluxes are given by $q^{(k)}(t,x) - u^{(k)}(t,x)p(u^{(k)}(t,x))$ which is the flux of the density, and $\dfrac{(q^{(k)}(t,x))^2}{u^{(k)}(t,x)} - q^{(k)}(t,x)p(u^{(k)}(t,x))$ which is the flux of the pseudo-momentum. Note that there is a negative sign in front of the flux term in Eq. (2.2), which comes from the position mapping $x \mapsto -x$ to update the computational domain from $[-1, 0]$ to $[0, 1]$ on the incoming roads. The initial

conditions for the density and pseudo-momentum are prescribed on each road with the functions $u_0^{(k)}$ and $q_0^{(k)}$, with the coupling conditions $\Phi(U^{(k)}(t, 0^+)) = 0$ defined for each set of PDEs and depends on *both* the incoming and outgoing roads, hence $k = 1, \ldots, m$.

2.2. Coupling conditions

Coupling conditions prescribe equations that must be satisfied at the junction. These conditions model conservation of quantities, determine how much flow moves from road to road, and how quantities can be maximized or minimized. Different coupling conditions for second-order models of traffic flow have been proposed in the literature [21,23,24], and all of the methods described above provide a unique solution to the Riemann problem at the junction. Below, we will review them individually. First, there are some coupling conditions that are accepted by all of the papers we consider. Those coupling conditions are:

- The flux of the density must be conserved. This condition is required, as the number of vehicles that enter the junction from incoming roads must leave on an outgoing road. That is, vehicles cannot be created or destroyed at the junction.
- Waves produced at the junction must have positive speed, assuming that we orient all roads out of the junction (see Fig. 2.1b). This consideration is taken so that the solution will satisfy the boundary conditions at the junction, and results in a physical model.

At this point we now review possible coupling conditions, as various authors have considered different possibilities at the junctions and the choice of coupling condition has been shown to slightly affect the solution determined by the method. In [21], the coupling conditions considered include, in addition to the two above, the following

- There exists a traffic distribution matrix A, stating what percentage of the flux of the density on each incoming road moves to each outgoing road.
- The sum of the flux of the density on incoming roads is maximized.
- In some situations, the four coupling conditions above do not provide a unique solution. The last condition employed can be either: (i) maximize velocity on outgoing roads, (ii) maximize density on outgoing roads, or (iii) minimize the total variation of density on outgoing roads. According to [21], the choice of any one of (i)-(iii) isolates a unique solution, although the unique solution for each coupling condition may not be the same.

This model can be applied to the general $\widetilde{m}$-incoming and $\widehat{m}$-outgoing roads case, with the restriction that $\widetilde{m} \geq \widehat{m}$ (except for the special case of 1-incoming and 2-outgoing roads).

The coupling conditions in [23] include, in addition to the canonical two, the following three rules

- The quantity $\frac{q}{u}$, which describes the "behavior" of drivers, must be the same before and after the junction.
- The sum of the flux of the densities on incoming roads is maximized.
- In some cases, the rules above do not provide a unique solution. The last condition is to maximize velocity on outgoing roads.

The coupling conditions in [23] are developed only for junction problems where there are $\widetilde{m}$-incoming roads and 1-outgoing road, and 1-incoming road and $\widehat{m}$-outgoing roads. Note that the conditions are very similar, but the coupling conditions in [23] include a different condition, which ensures the quantity $\frac{q}{u}$ is the same on each side of the junction. Note that this conservation is not the same as *conservation of the flow*, as the total flow of the quantity $\frac{q}{u}$ may not be the same on both sides of the junction. Instead, each vehicle tends to conserve their *quantity*, $\frac{q}{u}$, through the junction. Another distinct difference between the two sets of coupling conditions is the order in which variables are fixed or maximized on outgoing roads. In [23], maximization of the flux of the density is the final coupling condition implemented, whereas in [21] the maximization is the first coupling condition that is computed to set up a system of nonlinear equations. There are some important physical consequences of these choices.

Another set of coupling conditions given in [24] incorporate microscopic behavior at the junction to model junction merge behavior, and includes

- The flux of the pseudo-momentum q is conserved at the junctions.
- The sum of the flux of the densities on incoming roads is maximized, subject to a traffic distribution matrix A.
- In the case for 2 incoming roads and 1 outgoing road (or more generally when there is more than one incoming road), a "mixture rule" corresponding to microscopic considerations of how vehicles merge at the junction is introduced.

We do not discuss the details of [24] here, as we do not consider these coupling conditions in this paper. For the remainder of the paper, we only consider the sets of coupling conditions discussed in [21] and [23]. The reader interested in the microscopic considerations to derive macroscopic coupling conditions should refer to [24]. This concludes the discussion of the coupling conditions.

3. Discontinuous Galerkin (DG) method

3.1. Notation

Given an interval $I=[a,b]$, we divide I into N subintervals and label each cell as $I_j=[x_{j-\frac{1}{2}},x_{j+\frac{1}{2}}]$ for $j=1,\dots,N$, with $a=x_{\frac{1}{2}}$ and $b=x_{N+\frac{1}{2}}$. The center of each cell is given by $x_j=\frac{1}{2}(x_{j-\frac{1}{2}}+x_{j+\frac{1}{2}})$, with mesh size $h_j=x_{j+\frac{1}{2}}-x_{j-\frac{1}{2}}$. We denote the maximal mesh size as $h=\max\limits_{1\le j\le N} h_j$. Let V_h^κ denote the piecewise polynomial space

$$V_h^\kappa=\{v:\ v|_{I_j}\in P^\kappa(I_j),\ \ j=1,\dots,N\}, \tag{3.1}$$

where $P^\kappa(I_j)$ denotes the space of polynomials of degree κ on the cell I_j. Functions in V_h^κ are allowed to have discontinuities across the cell interface. The terms $v^-_{j+\frac{1}{2}}$ and $v^+_{j+\frac{1}{2}}$ represent the limit value of v at $x_{j+\frac{1}{2}}$ from the left cell I_j and the right cell I_{j+1}, respectively.

We let $U_h\in V_h^\kappa$ denote the solution of the DG numerical method. The notations for the jump at the interface, and the average of the function are given by $[U_h]=U_h^+-U_h^-$ and $\{U_h\}=\frac{1}{2}\left(U_h^++U_h^-\right)$, respectively. For shorthand notation, we define

$$(\phi,\psi)_{I_j}=\int_{I_j}\phi\psi\,dx, \qquad (\phi,\psi)=\sum_{j=1}^{N}\int_{I_j}\phi\psi\,dx. \tag{3.2}$$

3.2. DG method for the AR model on each road

In this section, we construct the DG method for (2.1) and (2.2) by discretizing the space with the DG method, and using strong stability preserving (SSP) Runge-Kutta (RK) methods in time. As the outgoing and incoming road cases are the same up to a sign difference, we will just consider the outgoing road formulation as the incoming road formulation can be defined similarly.

We can write (2.1) (and similarly (1.1)) in the following general form of a system of conservation laws

$$U_t+F(U)_x=0, \tag{3.3}$$

on each road, where $F(U)$ is the flux term. Utilizing the conservative form of the AR model, we have the following variables

$$U=\begin{pmatrix} u\\ u(v+p(u))\end{pmatrix}=\begin{pmatrix} u\\ q\end{pmatrix}, \qquad F(U)=\begin{pmatrix} uv\\ uv(v+p(u))\end{pmatrix}=\begin{pmatrix} q-up(u)\\ \dfrac{q^2}{u}-qp(u)\end{pmatrix}. \tag{3.4}$$

Using the variables in (3.4), we formulate the DG method for the system (2.1) and (2.2) as the following: find $U_h^{(k)}\in V_h^\kappa$, such that

$$\left(\left(U_h^{(k)}\right)_t,\phi_h\right)_{I_j}=\left(F(U_h^{(k)}),(\phi_h)_x\right)_{I_j}-\widehat{F}_{j+1/2}(U_h^{(k),-},U_h^{(k),+})\phi^-_{h,j+1/2}+\widehat{F}_{j-1/2}(U_h^{(k),-},U_h^{(k),+})\phi^+_{h,j-1/2}, \tag{3.5}$$

for all test functions $\phi_h\in V_h^\kappa$. The $\widehat{F}_{j+1/2}$ terms represent the numerical fluxes, which come from the boundary terms at each cell interface obtained from the integration by parts. There is not a unique choice of the numerical flux in general. For our numerical experiments, we will use the Lax-Friedrichs (LF) flux which is given by

$$\widehat{F}_{j+1/2}(U^{(k),-}_{h,j+1/2},U^{(k),+}_{h,j+1/2})=\frac{1}{2}(F(U^{(k),-}_{h,j+1/2})+F(U^{(k),+}_{h,j+1/2}))-\frac{\alpha}{2}(U^{(k),+}_{h,j+1/2}-U^{(k),-}_{h,j+1/2}), \tag{3.6}$$

where $\alpha=\max\limits_{U}\{|\lambda_1(U)|,|\lambda_2(U)|\}$ is the Lax-Friedrichs constant. The maximum can be taken globally (over the entire computational domain) or locally, leading to the LF or local LF flux. The $\lambda_j(U)$ are the eigenvalues of Jacobian matrix of $F(U)$, which are given by $\lambda_1(U)=v=\frac{1}{u}\left(q-u^{\gamma+1}\right)$ and $\lambda_2(U)=v-\gamma u^\gamma$. The framework presented in this paper can also be applied to other choices of numerical fluxes as well.

The discretization of the spatial domain using the DG method handles all of the numerical fluxes at the edge of each cell, but a problem arises for the flux $\widehat{F}_{1/2}$ of the very first cell, as this is where the junction is located. To determine the

flux $\widehat{F}_{1/2}$, we need to implement the appropriate coupling conditions as outlined in section 2.2. In the next section, we will explain in details how we numerically compute these fluxes at the junction.

Spurious artificial oscillations can appear near discontinuities in the numerical solution where shock-waves appear in hyperbolic problems. When such oscillations appear, total variation bounded (TVB) limiters can be applied to control these artifacts and to achieve total variation stability. The limiter should not change the cell averages when the limiter is applied, and the accuracy of the method for smooth solutions should remain the same. In this paper, we apply the TVB limiter outlined in [38].

The DG formulation (3.5) for the AR model is solved in time utilizing the SSPRK3 method [22], which is given as

$$\begin{aligned}
(U_h^{(k)})^{(1)} &= (U_h^{(k)})^i + \Delta t^i L\left((U_h^{(k)})^i\right)\\
(U_h^{(k)})^{(2)} &= \frac{3}{4}(U_h^{(k)})^i + \frac{1}{4}(U_h^{(k)})^{(1)} + \frac{1}{4}\Delta t^i L\left((U_h^{(k)})^{(1)}\right)\\
(U_h^{(k)})^{i+1} &= \frac{1}{3}(U_h^{(k)})^i + \frac{2}{3}(U_h^{(k)})^{(2)} + \frac{2}{3}\Delta t^i L\left((U_h^{(k)})^{(2)}\right),
\end{aligned} \tag{3.7}$$

where L represents the spatial operator, which denotes the right side of (3.5), and Δt^i is the numerical time step.

4. Implementation of the coupling conditions

In this section, we describe the implementation of the coupling conditions for the AR model on a network in the general case, by extending the first order method developed in [9] to the high order DG framework. We start with describing the main idea to evaluate the numerical flux on the junction. In subsection 4.1, the methodology to decide the admissible region is presented, the maximization of density flux coupling condition is discussed in subsection 4.2, and in the subsequent subsections 4.3-4.6 we provide the specific coupling conditions we implement for the 1-1, 1-2, 2-1, and 2-2 junction cases, respectively. Finally, in 4.7, we discuss the optimization algorithms used in solving the maximization/minimization problems.

On each road, we utilize the DG method (3.5) with the Lax-Friedrichs flux (3.6) for the spatial discretization, and SSPRK3 scheme (3.7) in time. To construct DG method for the AR model on a network, it requires the implementation of coupling conditions at the left hand boundary $x = 0$, in other words, we need to determine $\widehat{F}_{1/2}(U_{h,1/2}^{(k),-}, U_{h,1/2}^{(k),+}) = \widehat{F}_{1/2}((U_h^{(k)})_L, (U_h^{(k)})_R)$, with $(U_h^{(k)})_L$ and $(U_h^{(k)})_R$ denoting the left and right states at the junction on the kth road. Note that $(U_h^{(k)})_R$ is the numerical solution in the *first* cell and $(U_h^{(k)})_L$ is the numerical solution in the "ghost cell". In our problem, it needs to be solved from the coupling conditions at the junction. For the case with no junction involved, $(U_h^{(k)})_L$ comes from the given boundary condition.

To determine the unknown values of $(U_h^{(k)})_L$, and subsequently the flux $\widehat{F}_{1/2}((U_h^{(k)})_L, (U_h^{(k)})_R)$, we extend the technique developed in [9] for the first order finite difference method to the DG framework. First, the DG method (3.5) is rewritten as the following equivalent formulation

$$\begin{aligned}
\left(\left(U_h^{(k)}\right)_t, \phi_h\right)_{I_j} = &-\left(F(U_h^{(k)})_x, (\phi_h)\right)_{I_j} - \left(\widehat{F}_{j+1/2}(U_h^{(k),-}, U_h^{(k),+}) - F(U_{h,j+1/2}^{(k),-})\right)\phi_{h,j+1/2}^{-}\\
&+\left(\widehat{F}_{j-1/2}(U_h^{(k),-}, U_h^{(k),+}) - F(U_{h,j-1/2}^{(k),+})\right)\phi_{h,j-1/2}^{+},
\end{aligned} \tag{4.1}$$

by applying integration by parts. Note that this DG formulation (4.1) is introduced just to motivate our approach in determining $(U_h^{(k)})_L$ at the junction, and will not be used in our algorithm. All of the computation use the conventional form (3.5). By introducing the notation of "fluctuations"

$$\begin{aligned}
\left(D_{j+1/2}^{(k)}\right)^{-} &= \widehat{F}_{j+1/2}(U_h^{(k),-}, U_h^{(k),+}) - F(U_{h,j+1/2}^{(k),-}),\\
\left(D_{j-1/2}^{(k)}\right)^{+} &= -\widehat{F}_{j-1/2}(U_h^{(k),-}, U_h^{(k),+}) + F(U_{h,j+1/2}^{(k),+}),
\end{aligned}$$

the DG method becomes

$$\left(\left(U_h^{(k)}\right)_t, \phi_h\right)_{I_j} = -\left(F(U_h^{(k)})_x, (\phi_h)\right)_{I_j} - \left(D_{j+1/2}^{(k)}\right)^{-}\phi_{h,j+1/2}^{-} - \left(D_{j-1/2}^{(k)}\right)^{+}\phi_{h,j-1/2}^{+}. \tag{4.2}$$

When $\phi_h = 1$, it reduces to $(\overline{U_h^{(k)}})_t|_{I_j} = -\left(D_{j+1/2}^{(k)}\right)^{-} - \left(D_{j-1/2}^{(k)}\right)^{+}$, which shares the form of the residual distribution method [3]. At the junction, the fluctuations $\left(D_{1/2}^{(k)}\right)^{\pm}$ are defined by

$$\left(D_{1/2}^{(k)}\right)^{-} = \widehat{F}_{1/2} - F\left((U_h^{(k)})_L\right), \qquad \left(D_{1/2}^{(k)}\right)^{+} = -\widehat{F}_{1/2} + F\left((U_h^{(k)})_R\right),$$

and the $\left(D_{1/2}^{(k)}\right)^-$ term contains all information of backward moving waves at the interface of the cell. One of the main coupling conditions outlined in traffic flow is that only waves entering the junction (right-moving waves or waves with positive speed) are admissible, as outlined in section 2.2. Ideally, to satisfy the coupling condition of admissible waves, we would like to require that $\left(D_{1/2}^{(k)}\right)^- = 0$, as this would mean there would be no information traveling backwards into the junction. If the Godunov flux with the exact Riemann solver is employed at the junction (as in [2] for the LWR model), this condition will be satisfied exactly. With the choice of LF flux (or other numerical flux corresponding to different approximate Riemann solvers), this condition cannot be enforced exactly, instead we relax it to the minimization problem

$$\min_{(U_h^{(k)})_L} \sum_{k=1}^{m} \left|\left|\left(D_{1/2}^{(k)}\right)^- \left((U_h^{(k)})_L, (U_h^{(k)})_R\right)\right|\right|^2, \tag{4.3}$$

subject to the coupling conditions

$$\Phi\left((U_h^{(1)})_I, \ldots, (U_h^{(m)})_I\right) = 0, \tag{4.4}$$

where k indexes the road number, m is the total number of roads, and the unknowns $(U_h^{(k)})_L$ are the left states coming from the variables u_h and q_h in the ghost cell, $(U_h^{(k)})_R$ are the right states coming from the first cell inside the domain, and $(U_h^{(k)})_I = (U_h^{(k)})_I\left((U_h^{(k)})_L, (U_h^{(k)})_R\right)$ are the intermediate values at $x = 0$ by solving the Riemann problem with left and right values $(U_h^{(k)})_{L,R}$ approximately. We could choose the intermediate values as

$$(U_h^{(k)})_I\left((U_h^{(k)})_L, (U_h^{(k)})_R\right) = \frac{1}{2}\left((U_h^{(k)})_R + (U_h^{(k)})_L\right) - \frac{1}{2\alpha}\left(F\left((U_h^{(k)})_R\right) - F\left((U_h^{(k)})_L\right)\right). \tag{4.5}$$

For the LF flux used in this paper, the left-moving (backwards) fluctuation takes the form of

$$\left(D_{1/2}^{(k)}\right)^- = \frac{1}{2}\left(F\left((U_h^{(k)})_R\right) - F\left((U_h^{(k)})_L\right)\right) - \frac{\alpha}{2}\left((U_h^{(k)})_R - (U_h^{(k)})_L\right). \tag{4.6}$$

The solution of the minimization problem (4.3) and (4.4) produces the values $(U_h^{(k)})_L$ in the ghost cells. Therefore, once the optimization problem is solved, we have the last component (flux $\widehat{F}_{1/2}$) to update the numerical solution of the DG method (3.5) and (3.6) at the given time step.

In the following subsections, we consider the coupling conditions discussed in [21] and [23] which will be defined in (4.4) for the cases of 1-1, 1-2, 2-1, and 2-2 junction types, where the first number is the number of incoming roads and the second one is the number of outgoing roads. For the situation of the 1-1 junction and 1-2 junction, the coupling conditions from both papers appear to produce practically same result, which will be shown in section 5. The 2-1 and 2-2 junction cases are more complicated, as there is mixing from incoming roads to outgoing roads. The 2-1 junction case, as we shall see, will provide an example where the two sets of coupling conditions differ. The 2-2 case is only considered with the coupling conditions from [21], as the coupling conditions in [23] are only provided for the $\widetilde{m} - 1$ and $1 - \widetilde{m}$ junction types.

Before proceeding further, we give an overview of the procedure for the implementation of the coupling conditions. All of the coupling conditions, except for the maximization of density flux and preference for waves of positive speed, can be described via nonlinear algebraic equations. The two exceptions are formulated through optimization problems. The preference for waves of positive speed condition, when using the LF flux, is defined through the minimization of fluctuations (4.3), when solved will provide the unknown left states at the junction. Prior to being able to solve the minimization problem (4.3), the coupling conditions (4.4) must be defined as a system of equations, which requires the maximization of density flux problem to be solved beforehand. The maximization of the density flux problem returns the maximized fluxes which are used to construct nonlinear equations used in the definition of (4.4). To solve the maximization of density flux, we must first determine the admissible values for the flux of the density. The admissible values of the density flux must be consistent with the preference for waves of positive speed condition, which in turn is determined by the states in the ghost cells of the left states through the junction Riemann problem. For example, in [21], the admissible region for the flux of the density must be determined on each road, consistent with the coupling condition requirements. The admissible region is a function of $(U_h^{(k)})_R$ and γ in the (u, q)-plane with respect to some computed functions. The admissible region computation is also different for incoming and outgoing roads, therefore each case is treated separately.[4] It should be noted that the maximization problem may not return the maximum possible flux of the density, as heavily congested traffic will not allow for the maximum possible flux to be achieved. We now give the details of the admissible region in the next subsection, and those of the maximization of density flux in Section 4.2.

[4] The maximization of density flux is used for the 1-2, 2-1, and 2-2 junction cases. The 1-1 junction case is simple and does not require this additional condition to obtain a unique solution, whereas the other junction types will require this coupling condition.

4.1. Determining the admissible region

The computation of the admissible regions for the two types of coupling conditions considered in this paper are discussed in [21] and [23]. To demonstrate the computation of the admissible regions for the AR model, we provide an overview of sections 5.1 and 5.2 in [21].

First, define the following regions $\mathcal{D}$, $\mathcal{D}_1$ and $\mathcal{D}_2$ in the (u,q)-plane as

$$\mathcal{D}_1 = \left\{(u,q) \in \mathcal{D} \,\middle|\, q \geq (\gamma+1)u^{\gamma+1}\right\}, \tag{4.7}$$

$$\mathcal{D}_2 = \left\{(u,q) \in \mathcal{D} \,\middle|\, q \leq (\gamma+1)u^{\gamma+1}\right\}, \tag{4.8}$$

$$\mathcal{D} = \left\{(u,q) \in \mathbb{R}^+ \times \mathbb{R}^+ \,\middle|\, u^{\gamma+1} \leq q \leq u\right\}. \tag{4.9}$$

The domains in (4.7)-(4.9) are referred to as *domains of invariance*. With the assumption that $u \in [0, u_{\max} = 1]$, by the generalized Greenshields' Relation[5]

$$v_{\max}(u) = 1 - u^{\gamma}, \tag{4.10}$$

and the equation for pseudo-momentum $q = u(v + u^{\gamma})$, the bounds of the domain $\mathcal{D}$ in (4.9) are readily obtained. The domains in (4.7) and (4.8) are two subdomains of $\mathcal{D}$. The importance of these domains is theoretical in nature, in that any initial data for the Riemann problem that lies in these domains must have a solution in the domains. These regions are used in [21] to determine the solution to the maximization of density flux problem which is discussed in the next subsection.

In order to satisfy the coupling condition that the waves produced by the half-Riemann problem must have positive speed, we must enforce the admissible region Ω_k^{inc}, for the density flux δ_k on the incoming roads to be

$$\Omega_k^{\text{inc}} = \begin{cases} \left[0, \gamma\left(\frac{1}{\gamma+1}\right)^{\frac{\gamma+1}{\gamma}}\left(\frac{q_R^{(k)}}{u_R^{(k)}}\right)^{\frac{\gamma+1}{\gamma}}\right], & \text{if } (u_R^{(k)}, q_R^{(k)}) \in \mathcal{D}_2, \\ \left[0, q_R^{(k)} - \left(u_R^{(k)}\right)^{\gamma+1}\right], & \text{if } (u_R^{(k)}, q_R^{(k)}) \in \mathcal{D}_1. \end{cases} \tag{4.11}$$

For what is to follow in subsection 4.2, we introduce a new notation for the upper bounds of the admissible regions. We define

$$\delta_k^{\max} = \begin{cases} \gamma\left(\frac{1}{\gamma+1}\right)^{\frac{\gamma+1}{\gamma}}\left(\frac{q_R^{(k)}}{u_R^{(k)}}\right)^{\frac{\gamma+1}{\gamma}} & \text{if } (u_R^{(k)}, q_R^{(k)}) \in \mathcal{D}_2, \\ q_R^{(k)} - \left(u_R^{(k)}\right)^{\gamma+1} & \text{if } (u_R^{(k)}, q_R^{(k)}) \in \mathcal{D}_1, \end{cases} \tag{4.12}$$

where $\delta_k^{\max}$ represents the maximum possible density flux on incoming road k. The *maximum possible* flux does not necessarily mean that $\delta_k^{\max}$ will be achieved in the maximization of flux, as severe congestion could cause less than optimal flux at the junction.

Second, we determined the admissible region Ω_k^{out} for the density flux on outgoing roads. One function of importance is the curve of the second family (CSF) going through $(u_R^{(k)}, q_R^{(k)})$, given by $q = \frac{q_R^{(k)}}{u_R^{(k)}}u + u^{\gamma+1} - (u_R^{(k)})^{\gamma}u$. This curve is determine through analyzing the Riemann problem for the AR model (details are provided in [21]). Again, we must have waves produced by the half-Riemann problem to have positive speed, thus the admissible region Ω_k^{out}, for the density flux δ_k on the outgoing roads is

$$\Omega_k^{\text{out}} = \begin{cases} \left[0, \gamma\left(\frac{1}{\gamma+1}\right)^{\frac{\gamma+1}{\gamma}}\right], & \text{if CSF is completely in } \mathcal{D}_1, \\ \left[0, \frac{1}{u_R^{(k)}}\left(q_R^{(k)} - \left(u_R^{(k)}\right)^{\gamma+1}\right)\left(1 + \left(u_R^{(k)}\right)^{\gamma} - \frac{q_R^{(k)}}{u_R^{(k)}}\right)^{\frac{1}{\gamma}}\right], & \text{otherwise.} \end{cases} \tag{4.13}$$

[5] Density must always be non-negative, and a maximum density a road can handle gives an upper bound; for simplicity we take the upper bound to be unity. Along with the assumption that velocity is non-negative, and the maximum velocity is governed by, what is known in traffic flow theory as, generalized Greenshields' relation.

Similar to the incoming road case, the $\delta_k^{\max}$ for outgoing roads are defined as

$$\delta_k^{\max} = \begin{cases} \gamma \left(\dfrac{1}{\gamma+1} \right)^{\frac{\gamma+1}{\gamma}}, & \text{if CSF is completely in } \mathcal{D}_1, \\ \frac{1}{u_R^{(k)}} \left(q_R^{(k)} - \left(u_R^{(k)} \right)^{\gamma+1} \right) \left(1 + \left(u_R^{(k)} \right)^{\gamma} - \frac{q_R^{(k)}}{u_R^{(k)}} \right)^{\frac{1}{\gamma}}, & \text{otherwise.} \end{cases} \tag{4.14}$$

A similar analysis of the Riemann problem with the coupling conditions outlined in [23] is also done, except that the admissible regions give restrictions on the values of the density and pseudo-momentum. As the theory of admissible regions are not the main focus of this paper, we omit the details of the computations. The details are provided in [23]. With the admissible regions for the density flux δ_k on both incoming and outgoing roads, and the maximum possible fluxes, we now have all the components necessary to solve the maximization of density flux optimization problem.

4.2. Maximization of density flux

Before proceeding with the case-specific maximization problems, we provide a general overview of the maximization flux coupling condition, and how the condition fits into (4.4). First, we use the notation $\widehat{\delta}_k$ to represent the solution to the maximization of flux problem, which is the maximal *attained* (not necessarily the maximum possible) flow leaving the incoming road k. The value of $\widehat{\delta}_k$ has bounds such that $\widehat{\delta}_k \in [0, \delta_k^{\max}]$ is enforced, where $\delta_k^{\max}$ represents the maximum possible flux determined through the admissible region computation described in 4.1. The $\widehat{\delta}_k$ values for each road k are dependent upon the value of γ in the pressure term and the right and left states of the density and pseudo-momentum for each road. The solution of the maximization problem returns the $\widehat{\delta}_k$ for *incoming* roads. To get the fluxes $\widehat{\delta}_k$ for the outgoing roads, the traffic distribution matrix A is applied to the vector of $\widehat{\delta}_k$ for *incoming* roads. We then set up the equations that are nonlinear in $u_L^{(k)}$

$$q_I^{(k)} - (u_I^{(k)})^{\gamma+1} - \widehat{\delta}_k = 0,$$

for $k = 1, \ldots, m$, where $u_I^{(k)}$ and $q_I^{(k)}$ are given by the interface equation (4.5). The other coupling conditions are already provided in terms of nonlinear equations. Putting these coupling conditions in vector form, we get the coupling condition vector Φ in (4.4). We can now consider the specific maximization problems for the 1-2, 2-1, and 2-2 cases.

For the 1-2 junction case, the maximization of flux coupling condition is given by:

$$\widehat{\delta}_1 = \max_{\delta_1} \ \delta_1, \qquad \text{subject to } \begin{cases} \delta_1 & \in [0, \delta_1^{\max}] \\ A \cdot \delta_1 & \in [0, \delta_2^{\max}] \times [0, \delta_3^{\max}] \end{cases}, \tag{4.15}$$

where A is the exogenous traffic distribution matrix, and $\widehat{\delta}_1$ is the flux of the density on the incoming road which solves the maximization problem. Recall that the admissible regions $[0, \delta_k^{\max}]$ are, in general, a function of the right state $(U_h^{(k)})_R = (u_R^{(k)}, q_R^{(k)})^T$ and the value of γ, through the admissible region computation. To get the value for the outgoing roads, we just apply the traffic distribution matrix A to this vector:

$$[\widehat{\delta}_2, \widehat{\delta}_3] = A \cdot \left[\widehat{\delta}_1\right] = [\alpha_{1,2}, \alpha_{1,3}] \cdot \left[\widehat{\delta}_1\right] = \left[\alpha_{1,2}\widehat{\delta}_1, \alpha_{1,3}\widehat{\delta}_1\right], \tag{4.16}$$

which states that the fraction $\alpha_{1,2}$ vehicles from incoming road 1 travel to outgoing road 2, and the fraction $\alpha_{1,3}$ vehicles from incoming road 1 travel to outgoing road 3, such that $\alpha_{1,2} + \alpha_{1,3} = 1$.

The maximization of flux for 2-1 junction case is slightly more complicated. One can imagine a freeway merge where two different freeways merge into a single one, and if there is a large number of vehicles attempting to enter from each incoming road, congestion sets in and traffic backs up. We consider two possibilities depending upon the values of $\delta_1^{\max}, \delta_2^{\max}$, and $\delta_3^{\max}$ determined from the admissible region calculation. If $\delta_1^{\max} + \delta_2^{\max} < \delta_3^{\max}$, then there will not be severe congestion, as both incoming road fluxes can be maximal and the condition $\widehat{\delta}_1 + \widehat{\delta}_2 = \widehat{\delta}_3 \in [0, \delta_3^{\max}]$ will be satisfied. In this case, we simply have that $\widehat{\delta}_k = \delta_k^{\max}$ for $k = 1, 2$, and $\widehat{\delta}_3 = \widehat{\delta}_1 + \widehat{\delta}_2$. In terms of the traffic distribution matrix, which in this case is given by $A = [1, 1]$, all vehicles must travel through the junction to the outgoing road such that

$$\widehat{\delta}_3 = A \cdot \left[\widehat{\delta}_1, \widehat{\delta}_2\right]^T = [1, 1] \cdot \left[\widehat{\delta}_1, \widehat{\delta}_2\right]^T = \widehat{\delta}_1 + \widehat{\delta}_2. \tag{4.17}$$

If on the other hand, $\delta_1^{\max} + \delta_2^{\max} > \delta_3^{\max}$, then it may be the case that the sum of the fluxes on the incoming roads will be greater than road 3 can accommodate (i.e. $\delta_3^{\max}$), and the required condition in (4.17) may produce results where $\widehat{\delta}_3 \notin [0, \delta_3^{\max}]$ if we use the $\delta_k^{\max}$ for $k = 1, 2$. To remedy this situation, we introduce a fixed "merge coefficient" called q^*, which states that the percentage q^* of vehicles can enter from road 1 and $1 - q^*$ can enter from road 2. For our numerical experiments, we take the value of $q^* = \frac{1}{2}$, but other choices can be made. Now, the maximization of flux of the density can be given as

$$\widehat{\delta} = \left[\widehat{\delta}_1, \widehat{\delta}_2\right] = \max_{\delta_1,\delta_2} \ \delta_1 + \delta_2, \qquad \text{subject to} \begin{cases} \delta_1 \in [0, \delta_1^{\max}] \\ \delta_2 \in [0, \delta_2^{\max}] \\ \delta_1 + \delta_2 \in [0, \delta_3^{\max}] \\ \dfrac{\delta_1}{q^*} = \dfrac{\delta_2}{1-q^*} \end{cases}, \tag{4.18}$$

where $\left[\widehat{\delta}_1, \widehat{\delta}_2\right]$ are the flux of the densities on the 2 incoming roads which solves the maximization problem. We then apply (4.17) to get the other 2 fluxes.

Finally, the maximization of flux for 2-2 junction case is similar to the 1-2 junction case with an additional incoming road, and can be written as

$$\widehat{\delta} = \left[\widehat{\delta}_1, \widehat{\delta}_2\right] = \max_{\delta_1,\delta_2} \ \delta_1 + \delta_2, \qquad \text{subject to} \begin{cases} \delta_1 \in [0, \delta_1^{\max}] \\ \delta_2 \in [0, \delta_2^{\max}] \\ [\alpha_{1,1}, \alpha_{1,2}] \cdot [\delta_1, \delta_2]^T \in [0, \delta_3^{\max}] \\ [\alpha_{2,1}, \alpha_{1,2}] \cdot [\delta_1, \delta_2]^T \in [0, \delta_4^{\max}] \end{cases}, \tag{4.19}$$

where $\alpha_{i,j}$ are the entries of the 2×2 traffic distribution matrix A. Again, this optimization provides the values of $\widehat{\delta}_1$ and $\widehat{\delta}_2$, from which we apply A to get $\left[\widehat{\delta}_3, \widehat{\delta}_4\right]^T = A \cdot \left[\widehat{\delta}_1, \widehat{\delta}_2\right]^T$ for the other two roads.

4.3. 1 incoming road, 1 outgoing road

For the simple 1-1 junction case, we treat a single road as if there were a junction located on the interior of the said single road. We can compare the junction model directly to the case where we treat the 1-1 junction as a single interval, and just apply DG normally. Both methods should return the same solution, and this could be used as the first step to validate the junction model.

For the network case, we could implement the conservation of the flux of the density and obtain the unique solution as stated previously. We consider the following coupling conditions using the intermediate approximation values at the junction via (4.5), which is given as

$$\Phi = \begin{bmatrix} q_I^{(1)} - (u_I^{(1)})^{\gamma+1} - \left(q_I^{(2)} - (u_I^{(2)})^{\gamma+1}\right) \\ \dfrac{q_I^{(1)}}{u_I^{(1)}} - \dfrac{q_I^{(2)}}{u_I^{(2)}} \end{bmatrix} = \begin{bmatrix} 0 \\ 0 \end{bmatrix}, \tag{4.20}$$

where the first condition is the conservation of the flux of the density for the interface values, and the second one is the conservation of the quantity $\dfrac{q_I}{u_I}$ at the junction for each road. These two conditions are enough in the simple 1-1 junction case to provide a unique solution to the problem.

4.4. 1 incoming road, 2 outgoing roads

In the 1-2 case, six unknowns need to be determined, $u_L^{(k)}, q_L^{(k)}$, for $k = 1, 2, 3$. The admissible regions are first computed through the procedure outlined in section 4.1, from which we can determine the upper bound on the flux of the density for each road, denoted as $\delta_k^{\max}$ for $k = 1, 2, 3$. Then using the method outlined in 4.2, the equations for the maximization of flux can be determined. For the case of 1 incoming road and 2 outgoing roads we can define the coupling conditions Φ_1 from [21] as

$$\Phi_1 = \begin{bmatrix} q_I^{(1)} - (u_I^{(1)})^{\gamma+1} - \widehat{\delta}_1 \\ q_I^{(2)} - (u_I^{(2)})^{\gamma+1} - \widehat{\delta}_2 \\ q_I^{(3)} - (u_I^{(3)})^{\gamma+1} - \widehat{\delta}_3 \\ q_I^{(2)} - u_I^{(2)} \\ q_I^{(3)} - u_I^{(3)} \end{bmatrix} = \begin{bmatrix} 0 \\ 0 \\ 0 \\ 0 \\ 0 \end{bmatrix}. \tag{4.21}$$

The first three lines enforce the flux of the density being equal to the value determined from the maximization problem (4.15). The last two conditions enforce the maximization of speed on outgoing roads condition, which states that $q_I^{(k)} = u_I^{(k)}$ must hold for outgoing roads.

We also consider the coupling condition given in [23]. The maximization of density flux problem for this set of coupling conditions is slightly different in implementation than that of those developed for the conditions in [21]. For coupling

conditions in [23], we still compute an admissible region but the maximization problem is not implemented over the value δ_k, but instead its constituent components $q^{(k)}$ and $u^{(k)}$. That is to say, for the 1-2 case we have

$$\widehat{\delta}_1 = \max_{q^{(1)},u^{(1)}} q^{(1)} - (u^{(1)})^{\gamma+1}, \qquad \text{subject to } \begin{cases} (u^{(k)}, q^{(k)})^T \in \text{AdR}, & \text{for } k = 1, \dots, m \\ q^{(1)} - (u^{(1)})^{\gamma+1} = \sum_{k=2}^{3} q^{(k)} - (u^{(k)})^{\gamma+1} \\ \dfrac{q^{(1)}}{u^{(1)}} = \dfrac{q^{(2)}}{u^{(2)}} = \dfrac{q^{(3)}}{u^{(3)}} \equiv \widehat{\epsilon} \end{cases}, \tag{4.22}$$

where AdR is the admissible region for the density and pseudo-momentum (see [23] for details on the computation of the admissible region). The value of $\widehat{\epsilon}$ is defined to be $\dfrac{q}{u}$ which is determined through this optimization, so that the quantity is the same on each side of the junction. This value is then the *fixed* value of $\widehat{\epsilon}$, describing the behavior of drivers, which is used in the minimization of fluctuations problem. Once we have $\widehat{\delta}_1$, applying (4.16) determines $\widehat{\delta}_2$ and $\widehat{\delta}_3$.

Having the setup with the maximization of density flux complete, the coupling conditions (4.4) utilized in [23] are given as

$$\Phi_2 = \begin{bmatrix} q_I^{(1)} - \left(u_I^{(1)}\right)^{\gamma+1} - \widehat{\delta}_1 \\ q_I^{(2)} - \left(u_I^{(2)}\right)^{\gamma+1} - \widehat{\delta}_2 \\ q_I^{(3)} - \left(u_I^{(3)}\right)^{\gamma+1} - \widehat{\delta}_3 \\ \dfrac{q_I^{(1)}}{u_I^{(1)}} - \dfrac{q_I^{(2)}}{u_I^{(2)}} \\ \dfrac{q_I^{(1)}}{u_I^{(1)}} - \dfrac{q_I^{(3)}}{u_I^{(3)}} \\ \dfrac{q_I^{(1)}}{u_I^{(1)}} - \widehat{\epsilon} \end{bmatrix} = \begin{bmatrix} 0 \\ 0 \\ 0 \\ 0 \\ 0 \\ 0 \end{bmatrix}, \tag{4.23}$$

where we have added conditions 4 and 5 to enforce the conservation of the value of the quantity $\dfrac{q}{u}$ across the junction, and condition 6 to enforce the equality of $\dfrac{q}{u}$ with the fixed value of $\widehat{\epsilon}$.

4.5. 2 incoming roads, 1 outgoing road

In the 2-1 case, we also need to determine 6 unknowns, $u_L^{(k)}, q_L^{(k)}$, for $k = 1, 2, 3$. This situation is more complicated than the previous two, as there is mixing involved at the junction, since vehicles are entering from both incoming roads into a single outgoing road which can cause severe congestion. As with the 1-2 case, the admissible regions are first computed to determine $\delta_k^{\max}$, which was outlined in section 4.1. Using the method outlined in 4.2, we obtain the equations from the maximization of density flux condition. The coupling conditions Φ_1 can thus be defined from [21] as

$$\Phi_1 = \begin{bmatrix} q_I^{(1)} - (u_I^{(1)})^{\gamma+1} - \widehat{\delta}_1 \\ q_I^{(2)} - (u_I^{(2)})^{\gamma+1} - \widehat{\delta}_2 \\ q_I^{(3)} - (u_I^{(3)})^{\gamma+1} - \widehat{\delta}_3 \\ q_I^{(3)} - u_I^{(3)} \end{bmatrix} = \begin{bmatrix} 0 \\ 0 \\ 0 \\ 0 \end{bmatrix}, \tag{4.24}$$

where the first 3 conditions are enforcing the values of the flux of the density on each road to be that of the solution of the maximization problem (4.18). The last condition enforces the maximization of speed condition.

We can also implement the coupling conditions from [23], where the maximization problem is slightly different from that of the 1-2 junction case. The maximization problem in this case is defined as

$$\widehat{\delta}_3 = \max_{q^{(1),(2)},u^{(1),(2)}} \sum_{k=1}^{2} q^{(k)} - (u^{(k)})^{\gamma+1}, \qquad \text{subject to } \begin{cases} (u^{(k)}, q^{(k)})^T \in \text{AdR} \\ \frac{q^{(1)} - (u^{(1)})^{\gamma+1}}{\beta_1} = q^{(3)} - (u^{(3)})^{\gamma+1} \\ \frac{q^{(2)} - (u^{(2)})^{\gamma+1}}{\beta_2} = q^{(3)} - (u^{(3)})^{\gamma+1} \\ \dfrac{q^{(3)}}{u^{(3)}} = \beta_1 \dfrac{q^{(1)}}{u^{(1)}} + \beta_2 \dfrac{q^{(2)}}{u^{(2)}} \equiv \widehat{\epsilon} \end{cases}, \tag{4.25}$$

where the β_k are the coefficients from $\beta_k = \delta_k^{\max} / \sum_{j=1}^{2} \delta_j^{\max}$ for $k = 1, 2$, and AdR is the admissible region from [23]. From the definition of β_k, we can obtain the values for the maximized flux by $\widehat{\delta}_k = \beta_k \widehat{\delta}_3$ for $k = 1, 2$. Similar to the 1-2 junction case, define the coupling conditions Φ_2 from [23] as

$$\Phi_2 = \begin{bmatrix} q_I^{(1)} - (u_I^{(1)})^{\gamma+1} - \widehat{\delta}_1 \\ q_I^{(2)} - (u_I^{(2)})^{\gamma+1} - \widehat{\delta}_2 \\ q_I^{(3)} - (u_I^{(3)})^{\gamma+1} - \widehat{\delta}_3 \\ \beta_1 \dfrac{q_I^{(1)}}{u_I^{(1)}} + \beta_2 \dfrac{q_I^{(2)}}{u_I^{(2)}} - \dfrac{q_I^{(3)}}{u_I^{(3)}} \\ \dfrac{q_I^{(3)}}{u_I^{(3)}} - \widehat{\epsilon} \end{bmatrix} = \begin{bmatrix} 0 \\ 0 \\ 0 \\ 0 \\ 0 \end{bmatrix}, \tag{4.26}$$

where the first three conditions in Φ_2 correspond to conservation of the flux of the density, and the fourth and fifth representing the conservation of the quantity $\frac{q}{u}$ through the junction. The values of β_1 and β_2 are the coefficients describing what percentage of the flow into the outgoing road is coming from incoming road 1 and incoming road 2 which are defined after (4.25). The constants β_k essentially play the same role as q^* and $1 - q^*$ in (4.18), but do not necessarily have to be defined as *a priori* constants. For example, we could fix the β_k at the start of the implementation as constants, or define β_k as in the sum after (4.25). The choice is not unique as stated in [23]; the constants simply give preference to one road over another if $\beta_1 \neq \beta_2$ in the 2-1 junction case. These constants are introduced due to the possibility that the flow exiting the incoming roads is too great for the outgoing road to accept, which is why the introduction of these extra constants is required.

4.6. 2 incoming road, 2 outgoing roads

In the 2 incoming roads and 2 outgoing roads case, we must determine 8 unknowns, $u_L^{(k)}, q_L^{(k)}$, for $k = 1, 2, 3, 4$. The coupling conditions for the 2-2 junction case were only treated in [21], whereas the coupling conditions in [23] considered the $\widetilde{m} - 1$ and $1 - \widehat{m}$ junction cases only. So for this section we will only consider one set of coupling conditions, Φ.

For the case of 2 incoming roads and 2 outgoing roads we can define the coupling conditions as

$$\Phi = \begin{bmatrix} q_I^{(1)} - (u_I^{(1)})^{\gamma+1} - \widehat{\delta}_1 \\ q_I^{(2)} - (u_I^{(2)})^{\gamma+1} - \widehat{\delta}_2 \\ q_I^{(3)} - (u_I^{(3)})^{\gamma+1} - \widehat{\delta}_3 \\ q_I^{(4)} - (u_I^{(4)})^{\gamma+1} - \widehat{\delta}_4 \\ q_I^{(3)} - u_I^{(3)} \\ q_I^{(4)} - u_I^{(4)} \end{bmatrix} = \begin{bmatrix} 0 \\ 0 \\ 0 \\ 0 \\ 0 \\ 0 \end{bmatrix}, \tag{4.27}$$

where the first four equations are the result of the maximization problem (4.19), and the last two equations are the maximization of speed condition on the two outgoing roads. The traffic distribution matrix for the 2-2 junction case is given by

$$A = \begin{bmatrix} \alpha_{1,1} & \alpha_{1,2} \\ \alpha_{2,1} & \alpha_{2,2} \end{bmatrix},$$

where $\alpha_{1,1} + \alpha_{2,1} = 1 = \alpha_{1,2} + \alpha_{2,2}$. The relationship between the flux of the density at the junction is given by $\left[\widehat{\delta}_3, \widehat{\delta}_4\right]^T = A \cdot \left[\widehat{\delta}_1, \widehat{\delta}_2\right]^T$, where the $\widehat{\delta}_1$ and $\widehat{\delta}_2$ are the solutions to the maximization of the flow of the density on incoming roads condition, defined in (4.19).

4.7. Optimization problems

For the implementation of the coupling conditions described in this section, there are two optimization problems to be solved: the maximization problem in Subsection 4.2 which maximizes the flux of the density on incoming roads subject to various constraints, and the minimization of the fluctuations given by (4.3).

For the maximization problem, we use the `scipy.optimize.minimize` package in Python, where we implement the Sequential Least Squares Quadratic Programming (`SLSQP`) method [31,1]. The maximization problem involves maximizing an objective function subject to nonlinear equality constraints Φ, with bounds on the values of $u_L^{(k)}$ and $q_L^{(k)}$. Due

to the nonlinear equality constraints and bounds, the `SLSQP` solver can handle both constraints and bounds, and has also been robust in terms of initial conditions in all numerical tests for the maximization problem. Prior to the maximization of flux, we determine the admissible region for the flux of the density. The initial guess for the solver is taken to be the midpoint of the admissible region for the fluxes δ_1 and δ_2, depending on which junction case is being considered.

For the minimization problem (4.3), we implement the optimization algorithm via a Lagrange multiplier method described in [9]. The Armijo rule is utilized to determine the step size of the method. To simplify the notation, for the remainder of this subsection we drop the dependence on h and k so that $U_L = (U_h^{(k)})_L$. To solve (4.3), the Lagrange functional is defined as

$$\mathcal{L}(U_L, \mu) = g(U_L) + \mu^T \widetilde{\Phi}(U_L), \tag{4.28}$$

where

$$\begin{aligned} g(U_L) &= \sum_{k=1}^{m} \left|\left| \left(D_{1/2}^{(k)}\right)^{-} (U_L, U_R) \right|\right|^2, \\ \widetilde{\Phi}(U_L) &= \Phi(U_I(U_L, U_R)). \end{aligned} \tag{4.29}$$

At local minima the derivatives of (4.28) with respect to U_L and the Lagrange multipliers μ are equal to zero:

$$\begin{aligned} \nabla_\mu \mathcal{L}^T[\nu] &= \nu^T \widetilde{\Phi} = 0, \\ \nabla_{U_L} \mathcal{L}^T[\zeta] &= \nabla_{U_L} g^T \zeta + \mu^T \nabla_{U_L} \widetilde{\Phi} \zeta = 0. \end{aligned} \tag{4.30}$$

The first equation in (4.30) represents the coupling conditions, and the second equation in (4.30) is a linear system for the Lagrange multipliers μ. The system is overdetermined in this case as $c < mn$, where c is the number of coupling conditions. We can compute the minimizing solution for μ by the following equation

$$\mu = -\left(\nabla_{U_L} \widetilde{\Phi} \nabla_{U_L} \widetilde{\Phi}^T\right)^{-1} \nabla_{U_L} \widetilde{\Phi} \nabla_{U_L} g, \tag{4.31}$$

and the update for the values of the left-hand state in the ghost cells is given by

$$\widetilde{U}_L^{(i+1)} = U_L^{(i)} - \alpha \left(\nabla_{U_L} g + \nabla_{U_L} \widetilde{\Phi}^T \mu\right), \tag{4.32}$$

where the Lagrange multipliers are found via (4.31). The step size α can be determined through any line search algorithm, and the initial value $U_L^{(0)}$ is used to start the update step in (4.32), so that we can determine the temporary value of $U_L^{(i+1)}$, which we define as $\widetilde{U}_L^{(i+1)}$, such that the coupling conditions are satisfied, i.e. $\widetilde{\Phi}\left(\widetilde{U}_L^{(i+1)}\right) = 0$. Then we use the temporary value of $\widetilde{U}_L^{(i+1)}$ as the initial value for the minimization of $g(U_L)$ in (4.30), (4.3), and (4.4).

In the implementation for the initial condition of the solver, we define some vector ξ of pseudo-random numbers from a uniform distribution on either[6] $[-0.0001, 0.0001]$ or $[-0.001, 0.001]$, and define the initial value for the minimization problem as $U_L^0 = U_R^0 + \xi$, where U_R^0 is the vector of values of the states on right-hand side of the junction in the first cell of the domain.

In the numerical examples of Section 5, we use the Lagrange multiplier method as the optimizer of choice for the minimization problem (4.3). The optimizer has shown to be robust in finding local minima given our initial values, but is more time consuming than the `SLSQP` algorithm. For the `SLSQP` algorithm, we specify the objective function $g(U_L)$, its Jacobian, and the coupling conditions Φ as equality constraints as arguments to the solver, and the solver returns the U_L which minimize the objective function. We have chosen the Lagrange multiplier method for our numerical experiments due to the robustness on initial condition choice even though computation is more expensive. This is due to the fact that for some cases, the `SLSQP` method was sensitive to initial values for some junction types, and the method did not converge in all numerical experiments. When the `SLSQP` algorithm does converge, it is much faster than the Lagrange multiplier method, and converges to the same solution. As efficient treatment of optimization problems is not the goal of our paper, the Lagrange multiplier method has suited our needs for optimization. In any case, any choice of a nonlinear optimization solver that accepts bounds and constraints can be utilized here if speed is a concern.

5. Numerical experiments for the AR model

In this section numerical results are presented for the proposed DG method (3.5) for the AR model for different types of network junctions. In subsection 5.1, we present a convergence rate test to show the optimal convergence rate of the DG scheme for each polynomial space from P^0 to P^3 elements using coupling conditions from [21]. In subsection 5.2, we

[6] Numerical tests have shown nearly identical results, pulling ξ from either domain.

Table 5.1
Accuracy test for the system (1.3) with initial data (5.1) for the 1-1 junction case. The L^1 errors and orders for P^0, P^1, P^2, and P^3 solution spaces are given for the variables $u(x,T)$ and $q(x,T)$. Parameters: $\Delta x = 1/N$, $\Delta t = \text{CFL}\Delta x$, $T = 0.1$.

	N	j	$\|e^u\|_{L^1}$	Order	$\|e^q\|_{L^1}$	Order
P^0	10	0	1.2582e−02		1.2582e−02	
	20	1	6.3520e−03	0.98	6.3519e−03	0.98
	40	2	3.1976e−03	0.99	3.1975e−03	0.99
	80	3	1.6029e−03	0.99	1.6029e−03	0.99
	160	4	8.0250e−04	0.99	8.0250e−04	0.99
	320	5	4.0151e−04	0.99	4.0151e−04	0.99
P^1	10	0	5.8382e−04		5.8378e−04	
	20	1	1.4462e−04	2.01	1.4462e−04	2.01
	40	2	3.6042e−05	2.00	3.6042e−05	2.00
	80	3	9.0033e−06	2.00	9.0033e−06	2.00
	160	4	2.2503e−06	2.00	2.2503e−06	2.00
	320	5	5.6256e−07	2.00	5.6256e−07	2.00
P^2	10	0	3.1880e−05		3.1880e−05	
	20	1	4.7253e−06	2.75	4.7253e−06	2.75
	40	2	6.9243e−07	2.77	6.9243e−07	2.77
	80	3	1.0045e−07	2.78	1.0045e−07	2.78
	160	4	1.4417e−08	2.80	1.4417e−08	2.80
	320	5	2.0473e−09	2.81	2.0474e−09	2.81
P^3	10	0	4.4062e−07		4.4062e−07	
	20	1	2.5307e−08	4.12	2.5307e−08	4.12
	40	2	1.5541e−09	4.02	1.5541e−09	4.02
	80	3	9.6444e−11	4.01	9.6444e−11	4.01
	160	4	5.9881e−12	4.00	5.9881e−12	4.00
	320	5	3.8495e−13	3.95	3.8507e−13	3.95

consider the 1-1, 1-2, 2-1, and 2-2 junction types where we also consider coupling conditions provided in [21] for the AR model. The numerical results of the AR model plotted against the Godunov method for the LWR model (1.1), are also provided in this section, along with comparing the situation with different pressure terms for the AR model. Subsection 5.3 addresses the comparison of the different coupling conditions provided in subsection 2.2. Of special interest is subsection 5.3.3, where the numerical results are provided to support the case that capacity drop phenomenon can be observed with the second order AR model and the coupling conditions in [23].

5.1. Accuracy test

In this section, we test the accuracy of our proposed high order DG method (3.5), with the Lax-Friedrichs flux and the SSPRK3 temporal scheme (3.7). For the accuracy test, we take the CFL constant to be CFL = 0.1 for the P^0 and P^1 solution spaces, and CFL = 0.05 for the P^2 and P^3 solution spaces, so that the spatial error dominates for the higher order polynomial spaces. We then define the time step in terms of the spatial step size as $\Delta t = \text{CFL}\Delta x$. The accuracy test is based upon comparing the solution at consecutive mesh sizes and computing the L^1 error.

We consider the 1-1 junction case for the AR model (2.1) and (2.2), with coupling conditions given by (4.20), and the initial conditions given by

$$\begin{aligned} u_0(x) &= 0.5 + 0.25\cos(\pi x) \\ v_0(x) &= 1 - u_0(x). \end{aligned} \tag{5.1}$$

The computational domain is $[0,1]$ for the incoming road and outgoing road, where the junction is located at $x = 0$. The spatial mesh used for each P^κ is $\Delta x = \dfrac{1}{160}$, and periodic boundary conditions are implemented. The solutions are computed up to time $T = 0.1$. As seen in Table 5.1, we observe the (k+1)st order convergence rate of the DG method for P^κ ($\kappa = 0,1,2,3$) solution spaces for (3.5). The P^1_{ref} solution in Fig. 5.1 is obtained by using a refined mesh size of $\Delta x = 1/2560$, with the DG method implemented on a single continuous interval $[-1,1]$, with no junction.

5.2. Numerical experiments comparing LWR and AR models

In this section numerical results are presented for the proposed DG method (3.5) applied to AR model, and the DG method with the Godunov flux developed in [2] for the LWR models. In the first set of numerical test for each junction type, we do the same numerical test cases and initial conditions as in [2], to verify that the second order AR model can replicate the first order LWR model that was tested in the network case in [2]. Note that, if we take $v(t,x) = 1 - u(t,x)$ and

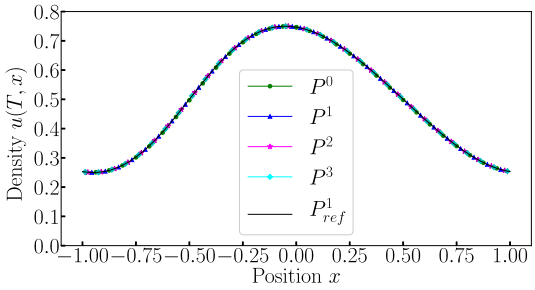

Fig. 5.1. One incoming and one outgoing road case with initial and boundary data given in (5.1). (For interpretation of the colors in the figure(s), the reader is referred to the web version of this article.)

$\gamma = 1$ in the pressure term $p(u) = u^\gamma$, the AR model reduces to the LWR model. We take these parameters for the first test case of each junction type.

To emphasize the difference between the LWR model and the AR model, we can then change the value of γ in the pressure term as is done in [30], which is carried out in subsection 5.2.4. The numerical experiments in [30] are for the single road Riemann problem case. In those examples, the velocity of vehicles in the AR model is shown to be faster than that of the LWR model. This behavior arises from an additional intermediate state that does not appear in the first order LWR model, which implies that the vehicles in the AR model have a less densely packed distribution than vehicles in the LWR model. Similar to the single road case, we consider the same type of approach in the network case. These numerical experiments are carried out for the cases of 2 incoming roads and 1 outgoing road.

5.2.1. One incoming road and two outgoing roads

In the first test with one incoming road and two outgoing roads, we use the following initial conditions

$$u_0^{(1)}(x) = 0.1, \tag{5.2}$$

$$u_0^{(2)}(x) = \begin{cases} 0.1, & \text{if } x \in [0, 0.2] \cup [0.4, 0.6] \cup [0.8, 1], \\ 0.2, & \text{otherwise}, \end{cases} \tag{5.3}$$

$$u_0^{(3)}(x) = 0.1, \tag{5.4}$$

with the coupling conditions given by (4.21), and with each road defined on the spatial interval $x \in [0, 1]$. The traffic distribution matrix is $A = [0.5, 0.5]^T$. We use the mesh size $\Delta x = 1/160$, and temporal step size $\Delta t = \text{CFL}\Delta x$, where CFL is the number given in Subsection 5.1 for each P^κ element space. The reference solution is obtained by running the Godunov method for the LWR model, as outlined in [2], with P^0 element and a spatial step size of $\Delta x = 1/5120$. The numerical results are given in Fig. 5.2, which shows that the proposed higher order DG scheme with the Lax-Friedrichs flux provides good numerical results and can resolve shocks and rarefactions well. Numerical results also demonstrate a good agreement with the reference solution computed by the method in [2] for the LWR model.

5.2.2. Two incoming roads and one outgoing road

For the next test with two incoming roads and one outgoing road, we use the following initial conditions

$$u_0^{(1)}(x) = \begin{cases} 0.1, & \text{if } x \in [0, 0.2] \cup [0.4, 0.6] \cup [0.8, 1], \\ 0.2, & \text{otherwise}, \end{cases} \tag{5.5}$$

$$u_0^{(2)}(x) = 0.1 + 0.05 \sin(5\pi x), \tag{5.6}$$

$$u_0^{(3)}(x) = 0.1, \tag{5.7}$$

with the coupling conditions given by (4.24), and with each road defined on the spatial interval $x \in [0, 1]$. We use the mesh size $\Delta x = 1/160$, and temporal step size $\Delta t = \text{CFL}\Delta x$. The reference solution is obtained by using the Godunov method for the LWR model, as outlined in [2], with P^0 element and a spatial step size of $\Delta x = 1/5120$. The results are given in Fig. 5.3. Similar to the 1-2 junction case, the numerical experiment shows that the higher order DG scheme again provides better numerical results than the first order methods, and agree well with the reference solution.

5.2.3. Two incoming roads and two outgoing roads

For the test with two incoming roads and two outgoing roads, we use the following initial conditions

$$u_0^{(1)}(x) = \begin{cases} 0.1, & \text{if } x \in [0, 0.2] \cup [0.4, 0.6] \cup [0.8, 1], \\ 0.2, & \text{otherwise}, \end{cases} \tag{5.8}$$

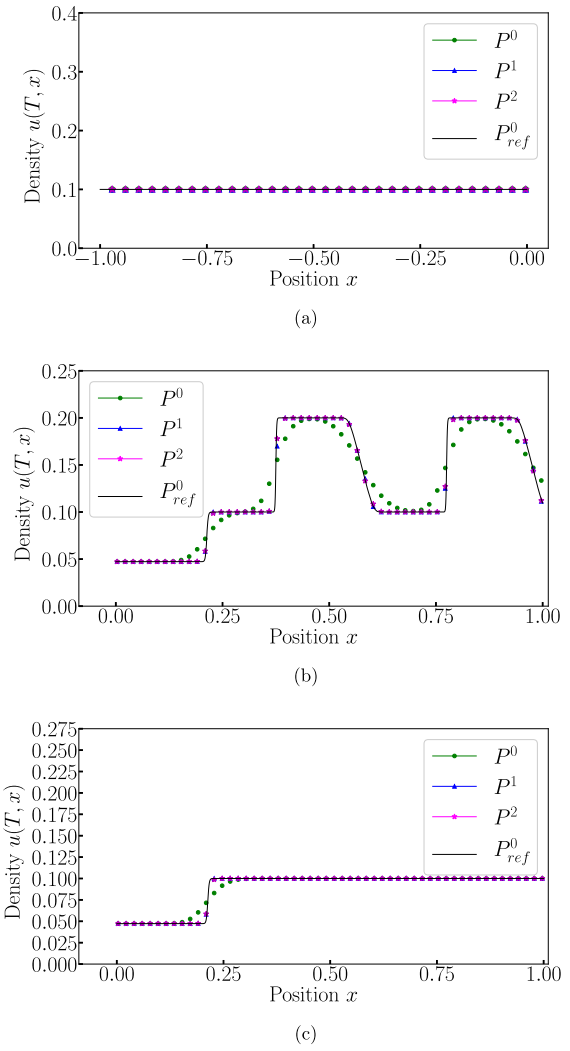

Fig. 5.2. One incoming and two outgoing roads with initial and boundary data (5.2)-(5.4), coupling condition (4.21), $\alpha = 0.5$, and $T = 0.25$. (a) Incoming Road 1; (b) Outgoing Road 2; (c) Outgoing Road 3.

$$u_0^{(2)}(x) = 0.2 + 0.1\sin(5\pi x), \tag{5.9}$$

$$u_0^{(3)}(x) = 0.5, \tag{5.10}$$

$$u_0^{(4)}(x) = 0.5, \tag{5.11}$$

with the coupling conditions given by (4.27), and with each road defined on the spatial interval $x \in [0, 1]$. The traffic distribution matrix that we use is given as

$$A = \begin{bmatrix} 0.4 & 0.3 \\ 0.6 & 0.7 \end{bmatrix}.$$

We use the mesh size $\Delta x = 1/160$, and temporal step size $\Delta t = \text{CFL}\Delta x$. The reference solution is obtained by using the Godunov method for the LWR model, as outlined in [2], with P^0 element and a spatial step size of $\Delta x = 1/5120$. The results are given in Fig. 5.4. In this more complicated situation, the higher order DG methods capture the complicated structure on the outgoing roads much better than the first order P^0 method, which exhibits numerical diffusion at the discontinuities. Again, our results agree well with the reference solution by the method in [2].

5.2.4. Two incoming roads and one outgoing road with different pressure terms

The goal of this test is to demonstrate the differences between the first order LWR model and second order AR model. We will use DG methods to solve both models. For the LWR model, the Godunov flux is used, and the Lax-Friedrichs flux

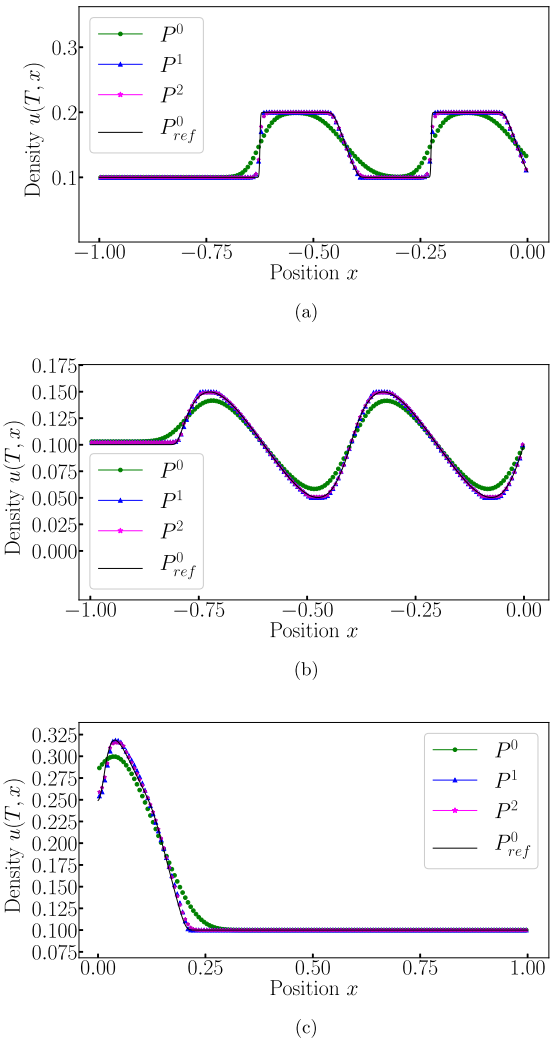

Fig. 5.3. Two incoming and one outgoing roads with initial data (5.5)-(5.7), coupling condition (4.24), and $T = 0.25$. (a) Incoming Road 1; (b) Incoming Road 2; (c) Outgoing Road 3.

is used for the AR model. Two cases of the AR model will be tested, one with $\gamma = 1$ and $\gamma = 2$, in the pressure term $p(u) = u^\gamma$. For the $\gamma = 1$ case, we will recover the LWR model as in the previous cases, while for $\gamma = 2$, we will observe the second order model effects. For this test with two incoming roads and one outgoing road, we use the following initial conditions

$$u_0^{(1)}(x) = \begin{cases} 0.5, & \text{if } x \in [0, 0.5], \\ 0.8, & \text{if } x \in (0.5, 1.0], \end{cases} \tag{5.12}$$

$$u_0^{(2)}(x) = u_0^{(1)}(x), \tag{5.13}$$

$$u_0^{(3)}(x) = u_0^{(1)}(x), \tag{5.14}$$

with the coupling conditions given by (4.24), and with each road defined on the spatial interval $x \in [0, 1]$. We use the P^2 element space, the mesh size $\Delta x = 1/160$, and temporal step size $\Delta t = 0.05\Delta x$. The DG method with P^0 element space is used for the LWR model, with a spatial step size of $\Delta x = 1/5120$. The results at $T = 0.15$ are given in Fig. 5.5 and the results at $T = 0.30$ are given in Fig. 5.6. The first row of figures gives the density profiles on each road, while the second row gives the velocity profiles on each road. The AR model with $\gamma = 1$ in the pressure term should recover the LWR model, and at both times $T = 0.15$ and $T = 0.30$, we see that the AR model recovers the LWR model well. When the AR model is used with $\gamma = 2$, we start to see the effects of using a second order model over the first order model. We can see that the density is more distributed over the incoming roads, and the speeds of the vehicles are greater. The behavior observed follows from the different wave speeds, which are affected by the pressure term in the AR model. The performance of the

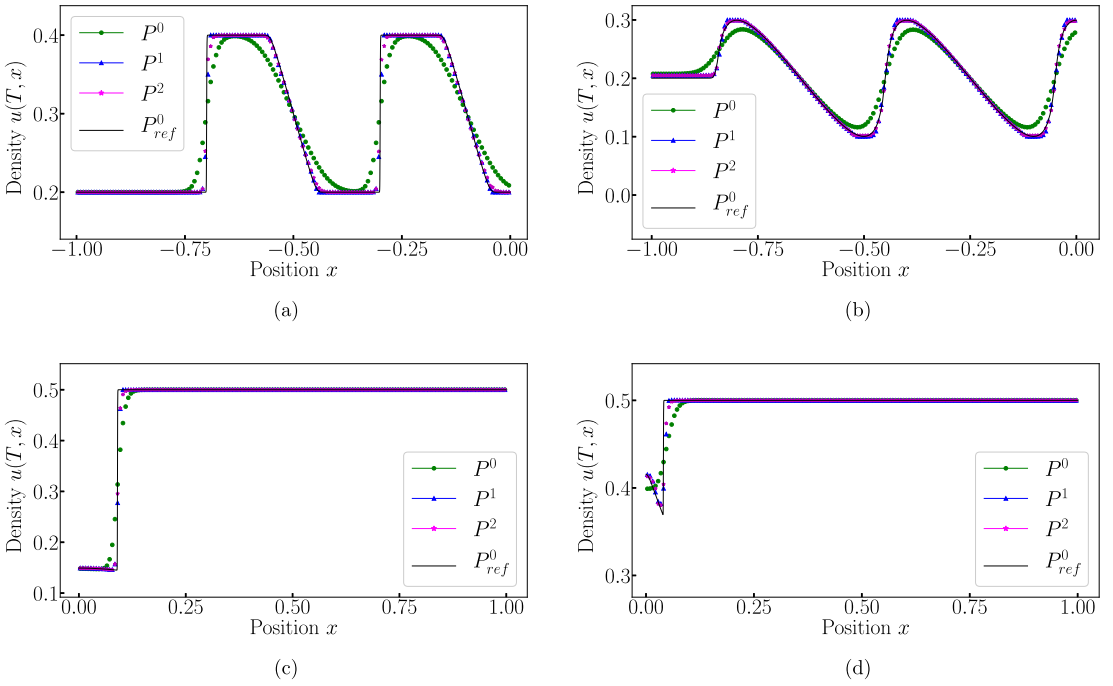

Fig. 5.4. Two incoming and two outgoing roads with initial data (5.8)-(5.11), coupling condition (4.27), and $T = 0.25$. (a) Incoming Road 1; (b) Incoming Road 2; (c) Outgoing Road 3; (d) Outgoing Road 4.

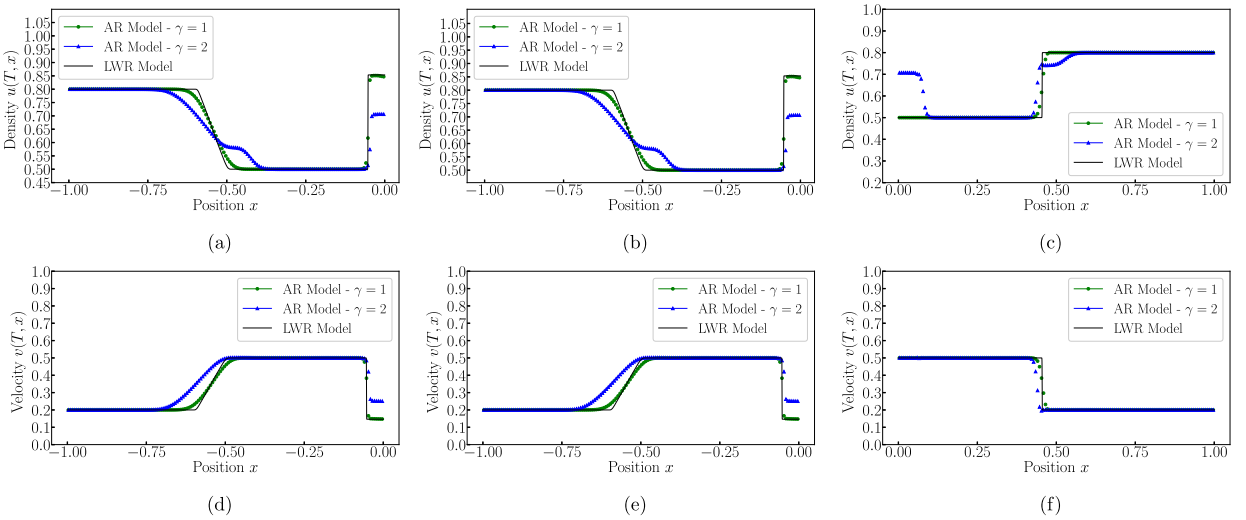

Fig. 5.5. Two incoming and one outgoing roads with initial data (5.12)-(5.14), coupling condition (4.24), and $T = 0.15$. (a) Incoming Road 1 density; (b) Incoming Road 2 density; (c) Outgoing Road 3 density; (d) Incoming Road 1 velocity; (b) Incoming Road 2 velocity; (c) Outgoing Road 3 velocity.

AR model in this numerical experiment agrees with the behavior outlined in [30], which reports similar results. Also of note in our junction model with the AR model case of $\gamma = 2$, the numerical experiment shows less congestion at the junction than the LWR case, as the density is distributed differently over the interval.

5.3. Comparisons of different coupling conditions

In this section numerical results are presented for the proposed DG method (3.5) applied to the AR model, with different types of coupling conditions in [21] and [23].

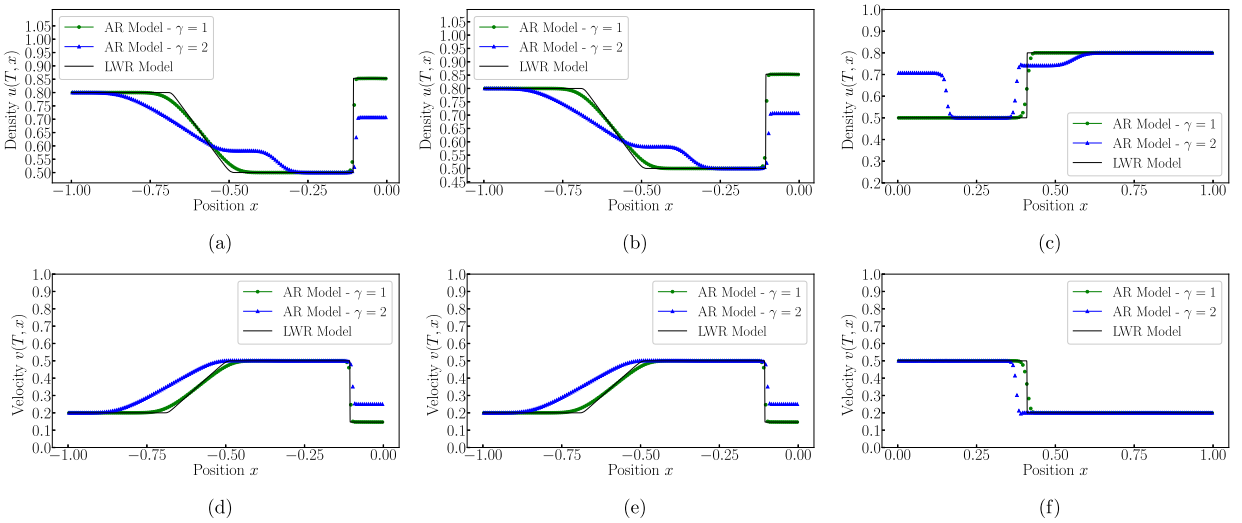

Fig. 5.6. Two incoming and one outgoing roads with initial data (5.12)-(5.14), coupling condition (4.24), and $T = 0.30$. (a) Incoming Road 1 density; (b) Incoming Road 2 density; (c) Outgoing Road 3 density; (d) Incoming Road 1 velocity; (b) Incoming Road 2 velocity; (c) Outgoing Road 3 velocity.

5.3.1. One incoming road and two outgoing roads

For the first test with one incoming road and two outgoing roads, we use the following initial conditions

$$u_0^{(1)}(x) = 0.1, \tag{5.15}$$

$$u_0^{(2)}(x) = \begin{cases} 0.1, & \text{if } x \in [0, 0.2] \cup [0.4, 0.6] \cup [0.8, 1], \\ 0.2, & \text{otherwise}, \end{cases} \tag{5.16}$$

$$u_0^{(3)}(x) = 0.1, \tag{5.17}$$

with the coupling conditions given by (4.21) (in [21]) and (4.23) (in [23]) to compare the effects of different coupling conditions. Each road defined on the spatial interval $x \in [0, 1]$. We use the mesh size $\Delta x = 1/160$, and temporal step size $\Delta t = \text{CFL}\Delta x$. The reference solution is obtained by using the Godunov method for the LWR model, as outlined in [2], with P^0 element and a spatial step size of $\Delta x = 1/5120$. The results are given in Fig. 5.7. The numerical results for both coupling conditions in this case are nearly identical, and both resolve the solution structure well for the high order method.

5.3.2. Two incoming roads and one outgoing road

For the next test with two incoming roads and one outgoing road, we use the following initial conditions

$$u_0^{(1)}(x) = 0.1 \tag{5.18}$$

$$u_0^{(2)}(x) = \begin{cases} 0.1 & \text{if } x \in [0, 0.2] \cup [0.4, 0.6] \cup [0.8, 1] \\ 0.2 & \text{otherwise}\ , \end{cases} \tag{5.19}$$

$$u_0^{(3)}(x) = 0.1 \tag{5.20}$$

with the coupling conditions given by (4.24) and (4.26). This test compares the effect of different coupling conditions. Each road defined on the spatial interval $x \in [0, 1]$. We use the mesh size $\Delta x = 1/160$, and temporal step size $\Delta t = \text{CFL}\Delta x$. The reference solution is obtained by using the Godunov method for the LWR model, as outlined in [2], with P^0 element and a spatial step size of $\Delta x = 1/5120$. The results are given in Fig. 5.8. As with the 1-2 junction case, the numerical results for both coupling conditions are nearly identical, and both are able to achieve good results with a complicated solution structure on the outgoing roads for the high order method.

The comparison of coupling conditions tests thus far appear to illustrate that the coupling conditions in [21] and [23] give similar, if not the same, numerical results. This can be explained by the fact that the initial conditions chosen for the numerical tests represent traffic conditions that do no introduce severe congestion at the junction. In the next subsection, we show that the coupling condition developed in [23] gives capacity drop when severe congestion is present, while the coupling condition in [21] does not generate the same results.

5.3.3. Capacity drop phenomenon test

In this subsection, we show the capacity drop phenomenon when applying the coupling conditions given in [23]. Capacity drop occurs when the outflow of vehicles from the junction is significantly lower than the maximum achievable flow at the

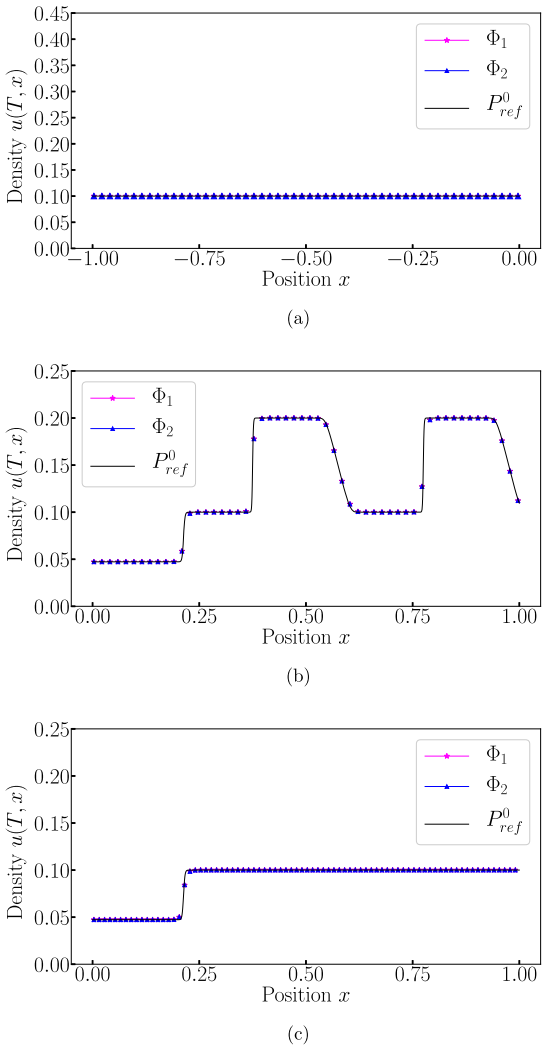

Fig. 5.7. Comparison of coupling conditions between [21] and [23]. One incoming and two outgoing roads with initial data (5.15)-(5.17), coupling conditions (4.21) and (4.23), $\alpha = 0.5$, and $T = 0.25$. (a) Incoming Road 1; (b) Outgoing Road 2; (c) Outgoing Road 3.

same location. Consider the 2-1 junction case. If the flow from the two incoming roads is large enough that the outgoing road cannot accommodate the incoming flows, the result is flows leaving incoming roads are lower than optimal, and the flow entering the outgoing road from the junction rises, then falls due to congestion. In [23], it is stated that the coupling conditions in (4.26) may be able to replicate the capacity drop phenomenon.

More recently, in [32] and [26], examples are constructed to show that the capacity drop phenomenon can be achieved. The papers also state that the choice of initial conditions are sensitive to the observation of the phenomenon, and observations made from real data should be used to calibrate the model. For our example, we follow the general method that is used in the previously mentioned papers to construct an appropriate initial condition. We will consider a constant density and velocity on Incoming Road 2 and Outgoing Road 3. We will then have density starting at a relatively low value and increase steeply, to overwhelm the outgoing road with an influx of vehicles, so that the resulting flow drops with an increase of density. As is done in [26], we track the density, density flux, and $w = q/u$ on Incoming Road 1, and density and density flux on Outgoing Road 3.

We implement the following initial conditions,

$$u_0^{(1)}(x) = \begin{cases} 0.1 + 0.7\sin\left(\frac{5}{2}\pi x\right), & \text{if } x \in [0, \zeta], \\ 0.4, & \text{for } x \in (\zeta, 1], \end{cases} \tag{5.21}$$

$$u_0^{(2)}(x) = 0.2, \tag{5.22}$$

$$u_0^{(3)}(x) = 0.1, \tag{5.23}$$

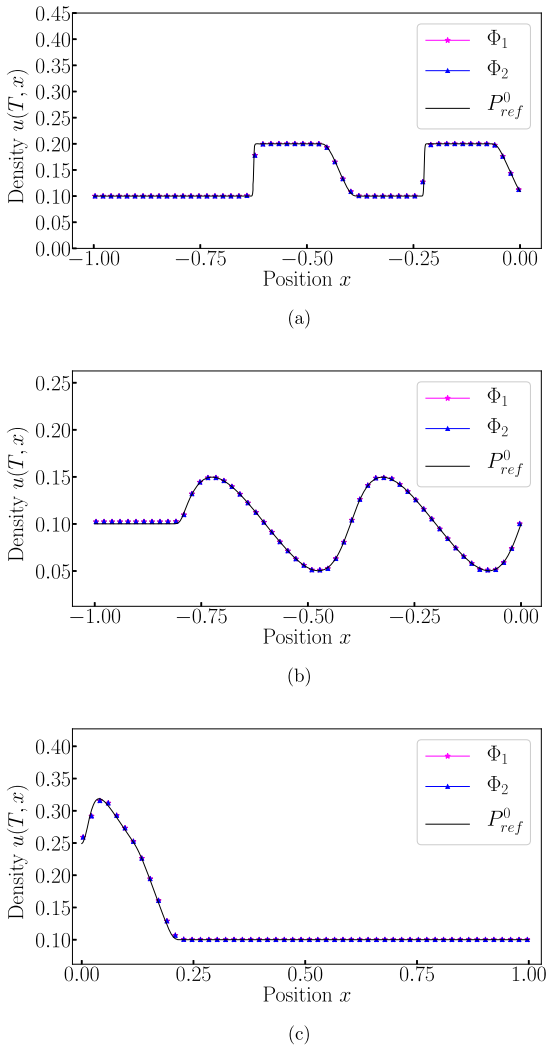

Fig. 5.8. Comparison of coupling conditions between [21] and [23]. Two incoming and one outgoing roads with initial data (5.18)-(5.20), coupling conditions (4.24) and (4.26), $\alpha = 0.5$, and $T = 0.25$. (a) Incoming Road 1; (b) Incoming Road 2; (c) Outgoing Road 3.

where $\zeta = 0.4 - \left(\frac{2}{5\pi}\right)\arcsin\left(\frac{3}{7}\right)$. For the velocity functions, we take $v_0(x) = 1 - u_0(x)$ as in the other numerical tests. The coupling conditions are given by (4.26), and with each road defined on the spatial interval $x \in [0, 1]$. We use the mesh size $\Delta x = 1/160$, and temporal step size $\Delta t = 0.05\Delta x$. The simulation is implemented up to $T = 0.655$, with $\gamma = 2$ in the pressure term, with P^2 elements. We also take $\beta_1 = \beta_2 = 0.5$ for the merge constants in the coupling conditions instead of the given definition, as is done in [26]. For comparison, we use the second set of coupling conditions (4.24) (in [21]) which do not give the capacity drop phenomenon.

The main numerical results to present the capacity drop pattern are provided in Fig. 5.10. The plots of the fluxes on Incoming Road 1 for the coupling conditions (4.26) and (4.24), are provided in Figs. 5.10a and 5.10b, respectively. Both sets of coupling conditions observe lower than optimal flux values entering the junction when congestion sets in, representing vehicles backing up on Incoming Road 1.

In Figs. 5.10c and 5.10d, the plots of the fluxes on Outgoing Road 3 are given for the coupling conditions (4.26) and (4.24), respectively. These plots support the conclusion that capacity drop is observed when using coupling conditions in (4.26). We observe that flow from the junction onto Outgoing Road 3 increases and then decreases once congestion sets in for the coupling conditions (4.26), whereas the coupling conditions in (4.24) have increasing flux and reach a near constant state. This behavior matches the capacity drop behavior which was reported in the discrete test case in [26]. Additionally, observe in Fig. 5.9, that density is non-decreasing and velocity is non-increasing over time. Also note that in Figs. 5.10e and 5.10f, that the quantity $w = q/u$ decreases, then increases slightly for the coupling conditions in (4.26) which have a change in driver behaviors due to the coupling condition involving the quantity $w = q/u$. In contrast, the coupling conditions in (4.24) have a near constant value. The final density profiles for each road at time $T = 0.655$ are given in 5.11. It is clear from

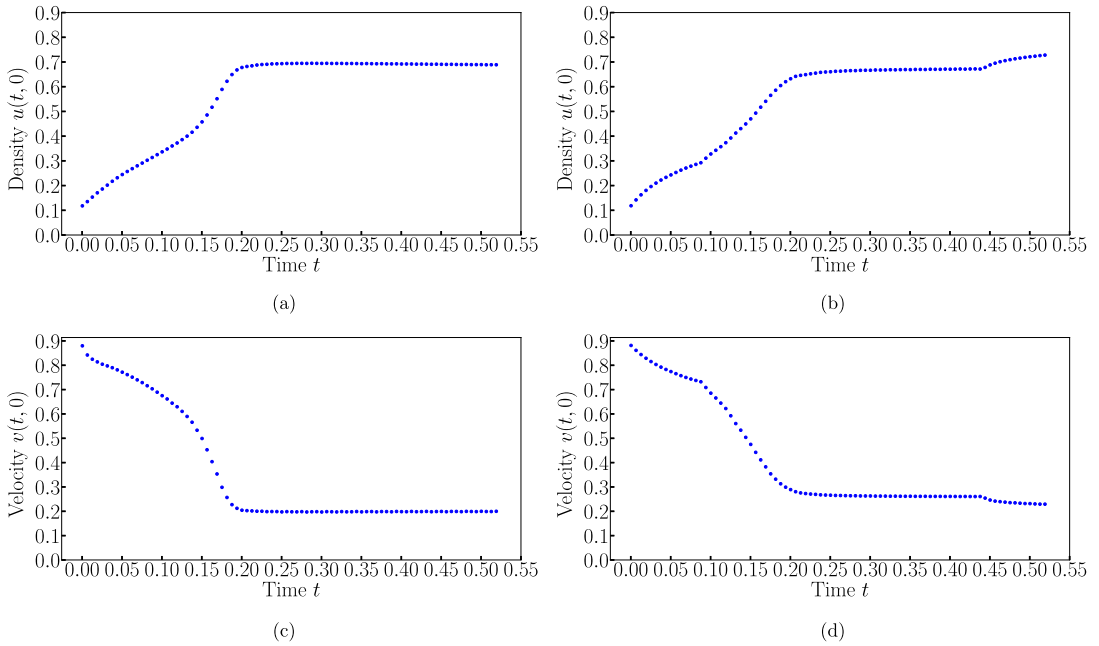

Fig. 5.9. Capacity drop test: density and velocity plots over time for the two incoming roads and one outgoing road case with initial data (5.21)-(5.23), coupling conditions (4.24) and (4.26), with P^2 elements, and $T = 0.655$. (a) Incoming Road 1 density over time with coupling conditions (4.26); (b) Incoming Road 1 density over time with coupling conditions (4.24); (c) Incoming Road 1 velocity over time with coupling conditions (4.26); (d) Incoming Road 1 velocity over time with coupling conditions (4.24).

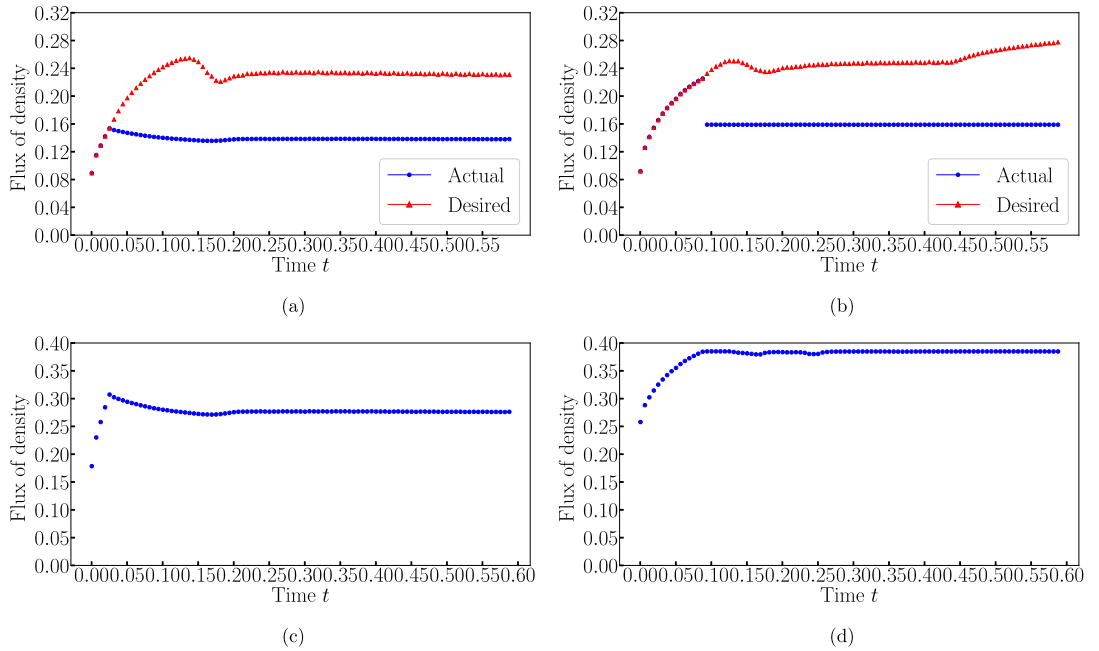

Fig. 5.10. Capacity drop test for two incoming roads and one outgoing road with initial data (5.21)-(5.23), coupling conditions (4.24) and (4.26), with P^2 elements, and $T = 0.655$. (a) Incoming Road 1 density flux with coupling conditions (4.26), with the blue curve representing $\widehat{\delta}_1$ and red curve representing $\delta_1^{\max}$ over time; (b) Incoming Road 1 density flux with coupling conditions (4.24), with the blue curve representing $\widehat{\delta}_1$ and red curve representing $\delta_1^{\max}$ over time; (c) Outgoing Road 3 density flux with coupling conditions (4.26); (d) Outgoing Road 3 density flux with coupling conditions (4.24); (e) Incoming Road 1 $w = v + p(u) = q/u$ with coupling conditions (4.26); (f) Incoming Road 1 $w = v + p(u) = q/u$ with coupling conditions (4.24).

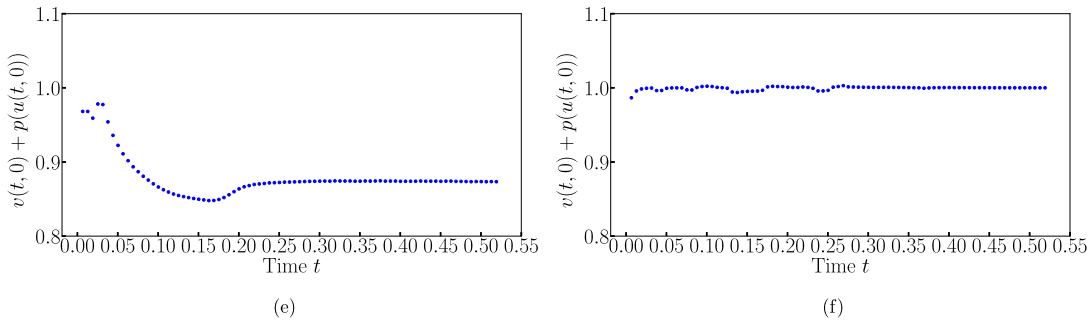

Fig. 5.10. (*continued*)

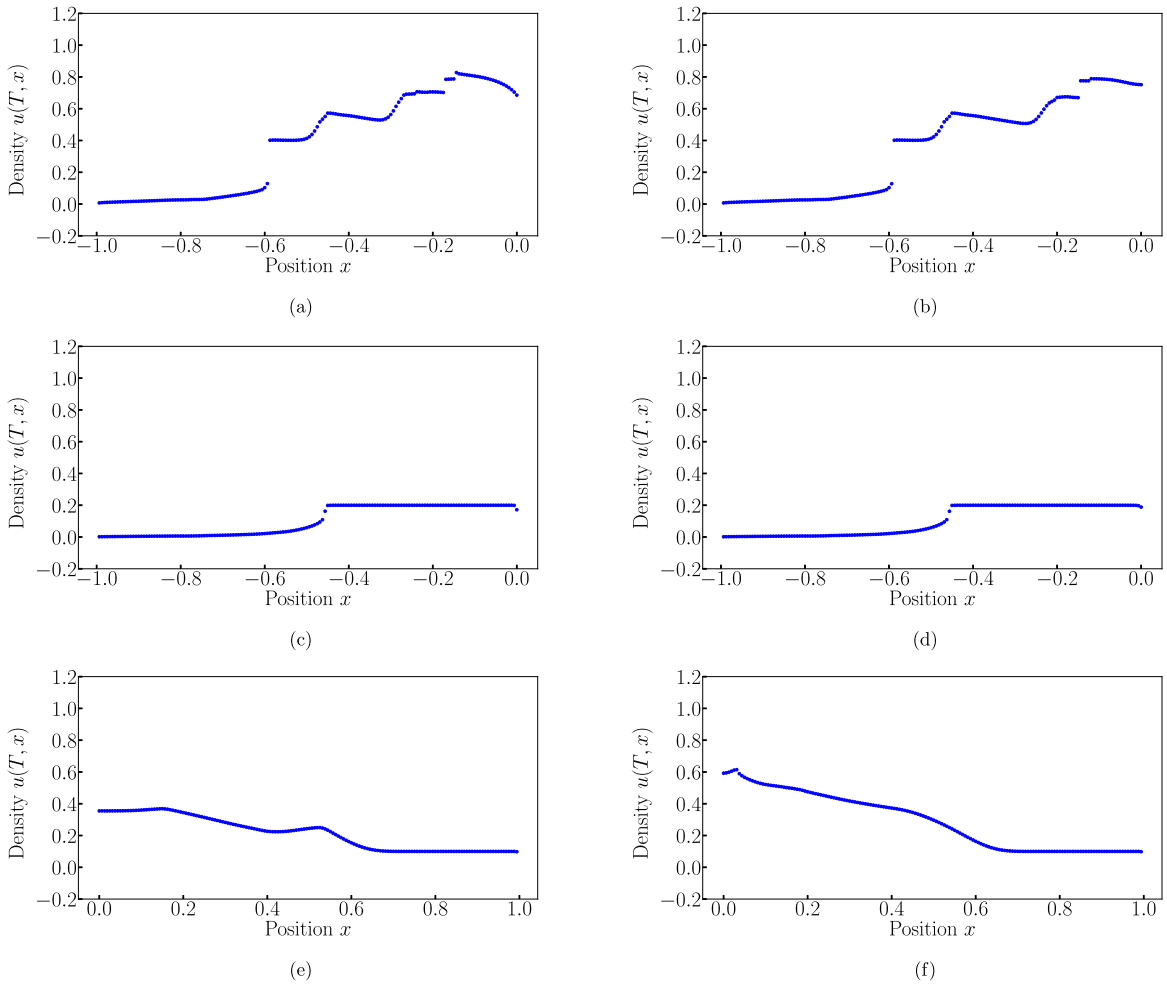

Fig. 5.11. Capacity drop test density profiles for two incoming roads and one outgoing road with initial data (5.21)-(5.23), coupling conditions (4.24) and (4.26), with P^2 elements, and $T = 0.655$. (a), (c), (e) Incoming Road 1, Incoming Road 2, Outgoing Road 3 densities with coupling conditions (4.26), respectively; (b), (d), (f) Incoming Road 1, Incoming Road 2, Outgoing Road 3 densities with coupling conditions (4.24), respectively.

this numerical test that the two sets of coupling conditions provide different results when severe congestion is introduced at the junction. We are also able to reproduce the capacity drop phenomenon for our continuous PDE based AR model using the DG method, and replicate similar qualitative results for the incoming and outgoing road quantities of the discrete test case reported in [26] which also observed capacity drop.

6. Conclusion

In this paper, we have constructed a general framework of DG methods to solve the AR model on networks (2.1) and (2.2). Arbitrary numerical flux can be used, which does not require the exact solution to the complicated Riemann problem, and in this paper we consider the Lax-Friedrichs flux as an example. This is an extension of the first order method developed in [9] for the junction problem to high order DG methods. Numerical examples are provided to demonstrate the high-order accuracy, and comparison of results between the first-order LWR model and the second-order AR model. The ability of the model to capture the capacity drop phenomenon is also explored. In future work, we hope to incorporate stochastic components which can be systematically added to the system, to determine if stochasticity can capture more complicated behavior seen in real traffic data. Another important avenue for extension is to use our proposed model to approximate traffic flow on a large network of connected junctions to model a real freeway system. This effort would implement the DG method via GPU parallelization to take advantage of the benefits of the DG method. PeMS data from Caltrans is open-source freeway sensor data that provides a jumping off point in evaluating the efficacy of our proposed method. Given the interest and availability of abundant data in today's world, analyzing data driven models for macroscopic PDE based methods would greatly benefit the traffic flow community in adopting these methods in practice.

Declaration of competing interest

The authors declare that they have no known competing financial interests or personal relationships that could have appeared to influence the work reported in this paper.

References

[1] Optimization (scipy.optimize), https://docs.scipy.org/doc/scipy/reference/tutorial/optimize.html, December 17, 2018.
[2] S. Čanić, B. Piccoli, J.-M. Qiu, T. Ren, Runge–Kutta discontinuous Galerkin method for traffic flow model on networks, J. Sci. Comput. 63 (1) (2015) 233–255.
[3] R. Abgrall, A review of residual distribution schemes for hyperbolic and parabolic problems: the July 2010 state of the art, Commun. Comput. Phys. 11 (4) (2012) 1043–1080.
[4] D. Armbruster, P. Degond, C. Ringhofer, A model for the dynamics of large queuing networks and supply chains, SIAM J. Appl. Math. 66 (3) (2006) 896–920.
[5] A. Aw, M. Rascle, Resurrection of "second order" models of traffic flow, SIAM J. Appl. Math. 60 (3) (2000) 916–938.
[6] M. Banda, A.-S. Häck, M. Herty, Numerical discretization of coupling conditions by high-order schemes, J. Sci. Comput. 69 (1) (2016) 122–145.
[7] F. Bellamoli, L. Müller, E. Toro, A numerical method for junctions in networks of shallow-water channels, Appl. Math. Comput. 337 (2018) 190–213.
[8] R. Biswas, K.D. Devine, J. Flaherty, Parallel adaptive finite element methods for conservation laws, Appl. Numer. Math. 14 (1994) 255–283.
[9] R. Borsche, Numerical schemes for networks of hyperbolic conservation laws, Appl. Numer. Math. 108 (2016) 157–170.
[10] A. Bressan, S. Čanić, M. Garavello, M. Herty, B. Piccoli, Flows on networks: recent results and perspectives, EMS Surv. Math. Sci. 1 (1) (2014) 47–111.
[11] M. Briani, B. Piccoli, J.-M. Qiu, Notes on RKDG methods for shallow-water equations in canal networks, J. Sci. Comput. 68 (3) (2016) 1101–1123.
[12] B. Cockburn, S. Hou, C.-W. Shu, The Runge-Kutta local projection discontinuous Galerkin finite element method for conservation laws IV: the multidimensional case, Math. Comput. 54 (1990) 545–581.
[13] B. Cockburn, G. Karniadakis, C.-W. Shu, The development of discontinuous Galerkin methods, in: B. Cockburn, G. Karniadakis, C.-W. Shu (Eds.), Discontinuous Galerkin Methods: Theory, Computation and Applications, in: Lecture Notes in Computational Science and Engineering, Part I: Overview, vol. 11, Springer, 2000, pp. 3–50.
[14] B. Cockburn, S.-Y. Lin, C.-W. Shu, TVB Runge-Kutta local projection discontinuous Galerkin finite element method for conservation laws III: one dimensional systems, J. Comput. Phys. 84 (1989) 90–113.
[15] B. Cockburn, C.-W. Shu, TVB Runge-Kutta local projection discontinuous Galerkin finite element method for conservation laws II: general framework, Math. Comput. 52 (1989) 411–435.
[16] C. Daganzo, The cell transmission model: a dynamic representation of highway traffic consistent with the hydrodynamic theory, Transp. Res., Part B, Methodol. 28 (4) (1994) 269–287.
[17] C. Daganzo, Requiem for second-order fluid approximations of traffic flow, Transp. Res., Part B, Methodol. 29 (4) (1995) 277–286.
[18] C. Daganzo, The cell transmission model, part II: network traffic, Transp. Res., Part B, Methodol. 29 (2) (1995) 79–93.
[19] C. Daganzo, N. Geroliminis, An analytical approximation for the macroscopic fundamental diagram of urban traffic, Transp. Res., Part B, Methodol. 42 (9) (2008) 771–781.
[20] C. D'Apice, R. Manzo, B. Piccoli, A fluid dynamic model for telecommunication networks with sources and destinations, SIAM J. Appl. Math. 68 (4) (2008) 981–1003.
[21] M. Garavello, B. Piccoli, Traffic flow on a road network using the Aw–Rascle model, Commun. Partial Differ. Equ. 31 (2) (2006) 243–275.
[22] S. Gottlieb, On high order strong stability preserving Runge Kutta and multi step time discretizations, J. Sci. Comput. 25 (1 and 2) (1999) 105–128.
[23] B. Haut, G. Bastin, A second order model of road junctions in fluid models of traffic networks, Netw. Heterog. Media 2 (2) (2007) 227.
[24] M. Herty, M. Rascle, Coupling conditions for a class of second-order models for traffic flow, SIAM J. Math. Anal. 38 (2) (2006) 595–616.
[25] H. Holden, N. Risebro, A mathematical model of traffic flow on a network of unidirectional roads, SIAM J. Math. Anal. 26 (4) (1995) 999–1017.
[26] O. Kolb, S. Göttlich, P. Goatin, Capacity drop and traffic control for a second order traffic model, Netw. Heterog. Media 12 (4) (2017) 663–681.
[27] M. Lighthill, G. Whitham, On kinematic waves II. A theory of traffic flow on long crowded roads, Proc. R. Soc. Lond., Ser. A, Math. Phys. Eng. Sci. 229 (1178) (1955) 317–345.
[28] P. Michalopoulos, D. Beskos, J.-K. Lin, Analysis of interrupted traffic flow by finite difference methods, Transp. Res., Part B, Methodol. 18 (4–5) (1984) 409–421.
[29] L. Müller, P. Blanco, A high order approximation of hyperbolic conservation laws in networks: application to one-dimensional blood flow, J. Comput. Phys. 300 (2015) 423–437.
[30] C. Niyitegeka, Numerical Comparisons of Traffic Flow Models, PhD thesis, Master's thesis, Department of Mathematics, TU Kaiserslautern and TU Eindhoven, 2012, VITA, 2002.
[31] J. Nocedal, S. Wright, Numerical Optimization, Springer, New York, 2006.

[32] C. Parzani, C. Buisson, Second-order model and capacity drop at merge, Transp. Res. Rec. 2315 (2012) 25–34.
[33] H. Payne, Models of freeway traffic and control, in: Mathematical Models of Public Systems, 1971.
[34] C. Puelz, S. Čanić, B. Rivière, C. Rusin, Comparison of reduced models for blood flow using Runge–Kutta discontinuous Galerkin methods, Appl. Numer. Math. 115 (2017) 114–141.
[35] W.H. Reed, T.R. Hill, Triangular Mesh Methods for the Neutron Transport Equation, Technical Report LA-UR-73-479, Los Alamos Scientific Laboratory, 1973.
[36] P. Richards, Shock waves on the highway, Oper. Res. 4 (1) (1956) 42–51.
[37] J. Sewall, D. Wilkie, P. Merrell, M. Lin, Continuum traffic simulation, Comput. Graph. Forum 29 (2) (2010) 439–448.
[38] C.-W. Shu, Discontinuous Galerkin methods: general approach and stability, in: Numerical Solutions of Partial Differential Equations, vol. 201, 2009.
[39] D. Sun, I. Strub, A. Bayen, Comparison of the performance of four Eulerian network flow models for strategic air traffic management, Netw. Heterog. Media 2 (4) (2007) 569.
[40] M. Zhang, C.-W. Shu, G. Wong, S. Wong, A weighted essentially non-oscillatory numerical scheme for a multi-class Lighthill–Whitham–Richards traffic flow model, J. Comput. Phys. 191 (2) (2003) 639–659.